WIND TURBINE CONTROL VIA POWER MEASUREMENTS IN COMPLEX TERRAIN

A Thesis Submitted to
the Graduate School of Engineering and Sciences of
İzmir Institute of Technology
in Partial Fulfillment of the Requirements for the Degree of

MASTER OF SCIENCE

in Energy Engineering

by
Deniz Gökhan DİRİK

December 2022
İZMİR

ABSTRACT

WIND TURBINE CONTROL VIA POWER MEASUREMENTS IN COMPLEX TERRAIN

This work presents an approach to the assessment of wind farm yaw control to utilize wake steering in complex terrain based on power measurements. Aerodynamic interactions between closely spaced wind turbines reduce the power output significantly. The standard wind turbine control strategy currently focuses on optimizing the wind turbines individually. However, there is growing evidence that these wake losses can be improved by optimizing for aerodynamic interactions between the turbines. In a case study, an assessment of wake steering gain and optimum yaw offset angles for each wind turbine are simulated for an operational wind farm. Wake losses are simulated for the wind farm and are validated using historical power measurements. Data analysis procedures for implementing operational wind farm data for the wake steering approach are described. Optimum yaw offset angles are calculated in simulations using operational data. A lookup table is generated for the optimum yaw angles required for each wind direction and speed bin. Using 5-year-long operational data, an average of 0.48% wake losses are calculated for the site. FLORIS simulations suggest 9.6% possible power improvement in wake losses using the optimum yaw offset angles. Using SCADA measurements for potential wake steering assessment allows rapid assessment and implementation without requiring expensive and year-long LIDAR or meteorological mast tower measurements.

ÖZET

KOMPLEKS ARAZİLERDE GÜÇ ÜRETİM ÖLÇÜMLERİYLE RÜZGAR TÜRBİNİ KONTROLÜ

Bu çalışma, rüzgar enerjisi santrallerinde yaw açısı kontrolü ile rüzgar izi rotasını kaydırmak için kompleks azilerde yapılan bir araştırmayı sumar. Birbirine yakın yerleşen rüzgar türbinlerinde aerodinamik etkileşimler sonucu önemli üretim kayıplar gerçekleşmektedir. Güncel rüzgar türbini kontrol stratejisi her bir türbinin kendi enerjisini maksimize edecek şekildedir. Modern literatürde rüzgar türbinlerinin kollektif kontrolünün, aerodinamik etkileşimler sonucu oluşan üretimi kayıplarını iyileştirebileceğine dair kanıtlar birikmektedir. Çalışma, operasyonel bir rüzgar enerjisi santralinde en elverişli yaw açısı sapmalarını bularak rüzgar izi rotasını kontrol etmeyi amaçlar. Rüzgar izi kayıpları simülasyonlar yardımı ile hesaplanmış ve operasyonel veriler ile teyit edilmiştir. Operasyonel veriler rüzgar izi rotasını saptırmak amacı ile analiz edilmiştir. Farklı atmosferik koşullarda, optimal güç üretimi için uygulanabilecek en iyi yaw açıları bulunmuştur. 5 yıllık operasyonel veri ile rüzgar izi kaynaklı yıllık ortalama %0.48 kayıp tespit edilmiştir. FLORIS simülasyonları ile optimum yaw açıları ile rüzgar izine bağlı kayıplarda teorik olarak %9.6 oranında bir iyileşmenin mümkün olduğu görülmüştür. SCADA ile kayıtlı ölçümlerin potensiyel rüzgar izi rotasını kaydırmak için maliyeti yüksek meteorolojik kule kurulumu ya da LIDAR ölçümlerine ihtiyaç duymadan hızlı bir şekilde değerlendirilebileceği gösterilmiş ve yöntemlerdeki belirsizlikleri azaltmak için öneriler sunulmuştur.

TABLE OF CONTENTS

LIST OF FIGURES

Figure **Page**

Figure **Page**

LIST OF TABLES

Table **Page**

CHAPTER 1

INTRODUCTION

Wind energy is critical in limiting the global warming and energy independence goals United Nations and energy policy advisors set. Renewable energy share in electrification is expected to grow from 26% in 2018 to 38% in 2030 without any intervention [1]. In line with the ambitious goals set by the United Nations Framework Convention on Climate Change (UNFCCC) and policy advisors IEC and IRENA for limiting global warming and energy independence, 56% of electrification is expected to be sourced from renewables by 2030 [1], [2]. Wind energy is expected to be one of the largest renewable energy providers. Even without the interventions like subsidization, certification of green resources, or carbon taxation, wind energy delivers one of the lowest Levelized Cost of Energy (LCOE) [3]. These ambitious goals depend on large deployments of wind energy clusters. Although wind atlas studies show great wind potential is available worldwide [4], the expansion of wind energy is primarily constrained by distance to the grid, proximity to residential areas, preserved areas, and social and political concerns. These economic, social, and political constraints require energy converters to use as little land as possible. However, Aerodynamic interactions between closely spaced wind turbines within a cluster reduce the power output significantly.

Currently deployed wind energy converters focus on optimizing individual turbine performance by tracking the optimal power point. However, there is growing evidence that wind farm production can be improved by optimizing for aerodynamic interactions between the turbines. To minimize the wake losses, multiple strategies have been suggested in the literature, including static or dynamic axial induction control [5], [6], wake redirection [7] or even repositioning offshore wind turbine depending on the seasonal winds. The most promising of these approaches has been wake steering with an increasing number of field studies [8] [9], as well as commercial adaptations of WindESCO Swarm [10], and Siemens Gamesa Wake Adapt [11].

This research focuses on the wake steering method in complex terrain based on operational data of a wind farm in Izmir, Turkey. First, wind energy principles from the perspective of wake steering are discussed in Chapter 1. In Chapter 2, data exploration, filtering, and analysis are presented for the five years long SCADA records and the nearby met mast measurements. Flow Redirection and Induction Steady State (FLORIS) [12] is used to simulate wake interaction between the wind turbines. It is shown that turbine level power measurements and FLORIS simulation agree on the wake losses. Optimal yaw offset angles are calculated using the FLORIS optimization toolbox, and the results are discussed in Chapter 3. Takeaways and recommendations on the subject are detailed in Chapter 4.

1.1 Wind Energy Principles

Wind energy is essentially the kinetic energy extracted from the wind. Wind turbine wake is the direct result of the turbine extracting the energy and leaving behind a low energy trail. Although fluid flow around a wind turbine is very complex, basic principles for extracting wind energy and wake effect can be modeled with an actuator disk normal to a uniform wind flow. Bernoulli equation is not valid for the whole streamtube due to pressure jump at an actuator disk. However, Bernoulli equations can be written for the streamtube in Figure 1.1 in two control volumes; upwind and downwind of the actuator disk.

Bernoulli equation at steady-state energy extraction for the streamtube with two control volumes with the inviscid, irrotational, incompressible, and conservative body forces assumptions can be written as;

$$p_{amb} + \frac{1}{2}\rho u_{amb}^2 = p_1 + \frac{1}{2}\rho u_1^2$$

$$p_2 + \frac{1}{2}\rho u_2^2 = p_{wake} + \frac{1}{2}\rho u_{wake}^2$$

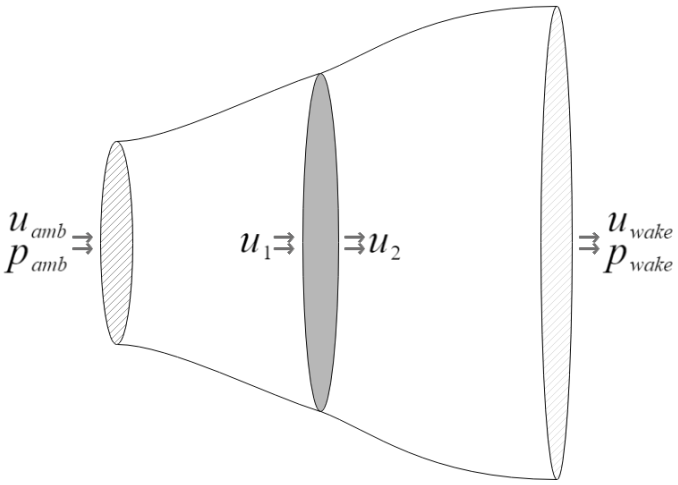

Figure 1.1: Streamtube around actuator disk of area A_r consisting of two control volumes; upwind region, before the actuator disk and the wake region, after the actuator disk.

where "$_{amb}$" subscripts denote ambient/freestream conditions. For far wake, wind flow will eventually recover; thus, $p_{wake} = p_{amb}$. Additionally, velocities before and after the actuator disk are equal, $u_1 = u_2 = u_r$. Combining two equations with these conditions,

$$p_1 - p_2 = \Delta p = \frac{1}{2}\rho(u_{amb}^2 - u_{wake}^2)$$

Then thrust on the actuator disk can be defined as,

$$T = A_r \Delta p = \frac{1}{2} A_r \rho (u_{amb}^2 - u_{wake}^2) \tag{1.1}$$

Additionally, due to mass conservation, $\dot{m} = \rho u_{amb} A = \rho u_{wake} A_{wake} = \rho u_r A_r$

$$T = \dot{m}(u_{amb} - u_{wake}) = \rho u_r A_r (u_{amb} - u_{wake}) \tag{1.2}$$

Then, combining 1.1 and 1.2, the velocity available at the actuator disk is,

$$u_r = \frac{u_{amb} + u_{wake}}{2}$$

A dimensionless axial induction factor a is commonly defined for representing

normalized velocity deficit from freestream wind speed u_{amb} to the rotor wind speed u_r

$$a = \frac{u_{amb} - u_r}{u_{amb}} \tag{1.3}$$

Then,

$$u_r = u_{amb}(1 - a)$$
$$u_{wake} = u_{amb}(1 - 2a)$$

And power and thrust can be more elegantly defined in terms of axial induction factor, as,

$$T = \frac{1}{2}\rho A_r u_{amb}^2 4a(1 - a)$$
$$P = \frac{1}{2}\rho A_r u_{amb}^3 4a(1 - a)^2$$

Total power and thrust available in the wind crossing rotor area is,

$$T_{wind} = \frac{1}{2}\rho A_r u_{amb}^2 \tag{1.4}$$
$$P_{wind} = \frac{1}{2}\rho A_r u_{amb}^3 \tag{1.5}$$

Commonly power coefficient of a wind turbine, C_p, is used to represent the ratio of power extracted from the wind and can be written in terms of axial induction factor,

$$C_p = \frac{P_{turbine}}{P_{wind}} = 4a(1 - a)^2$$

Similarly, the thrust coefficient of a wind turbine is,

$$C_t = \frac{T_{turbine}}{T_{wind}} = 4a(1 - a) \tag{1.6}$$

Additionally, investigating the critical points of C_p, it has a local maximum at a=1/3 in 0<a<1, and the maximum obtainable power is $C_p = 16/27$. The renowned Betz limit shows the maximum limit at which kinetic energy can be extracted from the wind.

The power and thrust output of a wind turbine can also be written in terms of power and thrust available in the wind in Equation 1.4, scaled by the utilization factors C_p and C_t, as,

$$P = \frac{1}{2}\rho A_r u_{amb}^3 C_p$$
$$T = \frac{1}{2}\rho A_r u_{amb}^2 C_t \tag{1.7}$$

Derivation of wind turbine power coefficient helps describe the energy extraction, resulting wake, and analytical models. However, turbine manufacturers must empirically represent the power and thrust coefficients according to the IEC standard 61400-12-1 [13]. The standard details how data should be collected to represent wind turbine performance in terms of C_p and power curve. Measurement-driven wind turbine characteristics are crucial for decision-making and siting. Although IEC standards represent the performance of a wind turbine in generic, unobstructed, and flat terrain conditions, detailed conversion methods are available in IEC 61400-1 [14] to enable the extension of the OEM power performance characteristics to site-specific conditions. Gathering year-long site conditions are required for wind farm planning and siting. These measurements are generally wind speed and direction, wind shear, temperature, and air density, collected at hub height using a meteorological mast tower. For this study, the power curve of each wind turbine is calculated using the 5-year-long operational data, and the methods are discussed in Section 2.2

1.2 Wind Turbine Structure

Modern wind energy converters extract the wind using 3-bladed, horizontal axis, variable speed, pitch-controlled wind turbines. Blades transfer the wind energy to the drive train. Transferred aerodynamic thrust is directly related to the wind speed, blade aerodynamics (including pitch), tip speed ratio, and yaw alignment to wind direction. Since wind turbines rotate much slower than the grid frequency of 50-Hz, either a gearbox is used to increase rotational speed or a high number of pole pairs are used in the generator for gearless wind converters. Wind energy fluctuates rapidly; therefore, power supplied to the grid should be decoupled from the generation. This is generally achieved using a combination of generators, rectifiers - dc-link - inverter units, and filters. In this study, wind energy converters at the experiment site were variable-speed, pitch-controlled, direct drive (gearless), and low-rotational-speed synchronous annular generators. The described structure is summarized in Figure 1.3.

A generic gearless wind turbine hub components are given in 1.2

1. Slip ring: allows power transmission in rotating structures,
2. Blade hub: binds the blades and the hub.
3. Pitch actuator: regulates wind extraction.
4. Stator: stationary part of the generator.
5. Rotor: rotary part of the generator.
6. Shield: shields the nacelle from the generator.

7-10. Rectifier, filter, excitation controller, and converter: power electronics.

11. Yaw actuators: rotate the nacelle to the wind direction.
12. Nacelle: Houses wind turbine components on the tower.

13-14. Blade extension and blade: extract the kinetic energy from wind/

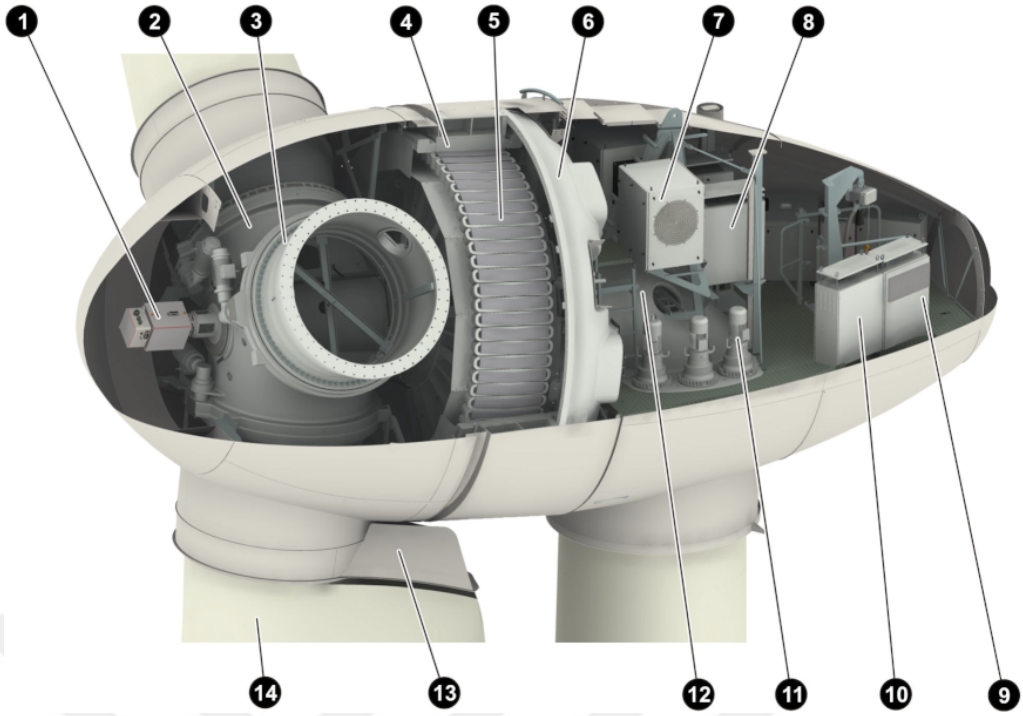

Figure 1.2: Wind turbine components. [15]

1.2.1 Wind Turbine Control

This section defines the wind turbine control for gathering maximum kinetic energy from the wind flow and wind turbine degrees-of-freedom, not the electrical control of the wind converter units. Mainly there are two controls for the wind flow. First is the wind turbine yaw control, which tracks the mean wind direction so that the rotor area is normal to the wind for optimum energy transfer. Second is the stall regulation which enables the wind turbine to continue operation after nominal wind speed is reached.

Pitch-regulated wind turbines adjust pitch angles to regulate the amount of wind energy extraction by changing the angle of attack on the blades. Pitch control is analogous to the governer control in traditional generator units, which controls the amount of fuel fed into the engine or water fed into a hydropower plant.

When available power in the wind exceeds the nominal capacity of the generator speed, kinetic energy extraction should be "stalled" to not exceed the rated generator power. Stall regulation can be achieved with pitch control or the aerodynamical design of wind turbine blades. Modern wind turbines mostly take the pitch control approach since

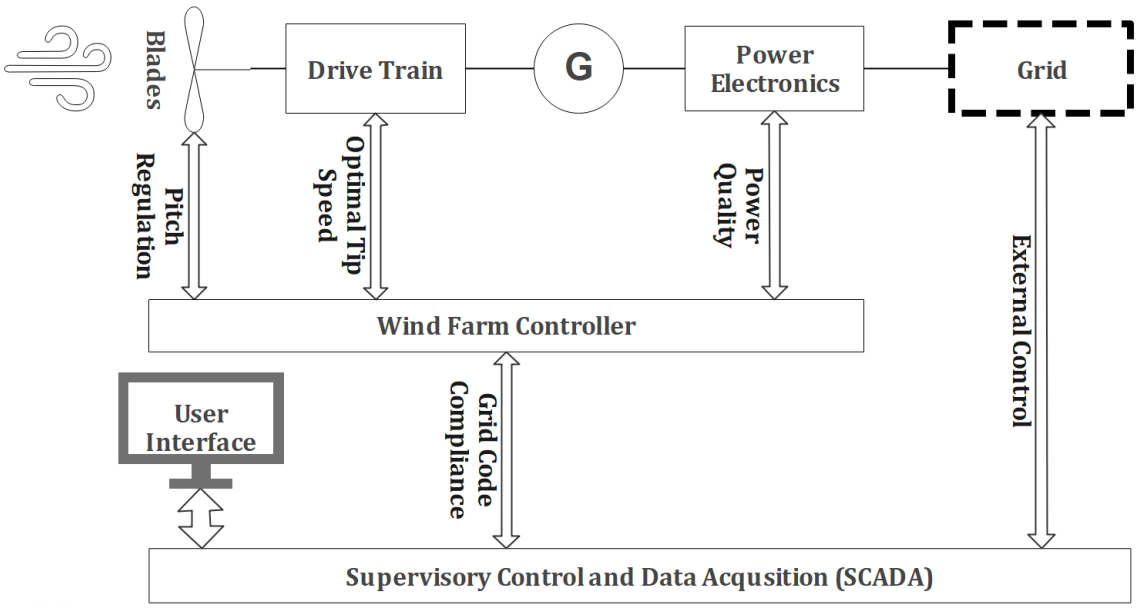

Figure 1.3: Wind turbine energy conversion process.

it allows the following points:

- Parking the wind turbines allows the minimum load on the structure where the rotor can rotate at very slow speeds. This allows the minimum load after cut-out wind speeds and during extreme atmospheric conditions. The maximum pitch position is set, resulting in the minimum lift at the blades.

- Reduce load when available power in the wind is higher than the nominal power of the wind energy converter. This allows the wind turbine to continue production after reaching the nominal speed.

- Can be used as an alternative to torque control to reduce power extraction and operate at an external set-point.

Torque and pitch control mechanisms are activated depending on the operation region in Figure 1.4. The list of operating regions depending on wind speed are:

- In region 1, wind speed is below cut-in speed, no electrical torque is present, and the pitch angle is set to a moderate value to minimize the load while being able to spin idly. Once the cut-in wind speed is reached, the generator is initially excited with power taken from the grid, and the turbine starts operation.

- In region 2, the wind turbine will try to track the optimal tip speed ratio by adjusting rotor torque to aerodynamically available torque. The pitch angle is minimized to

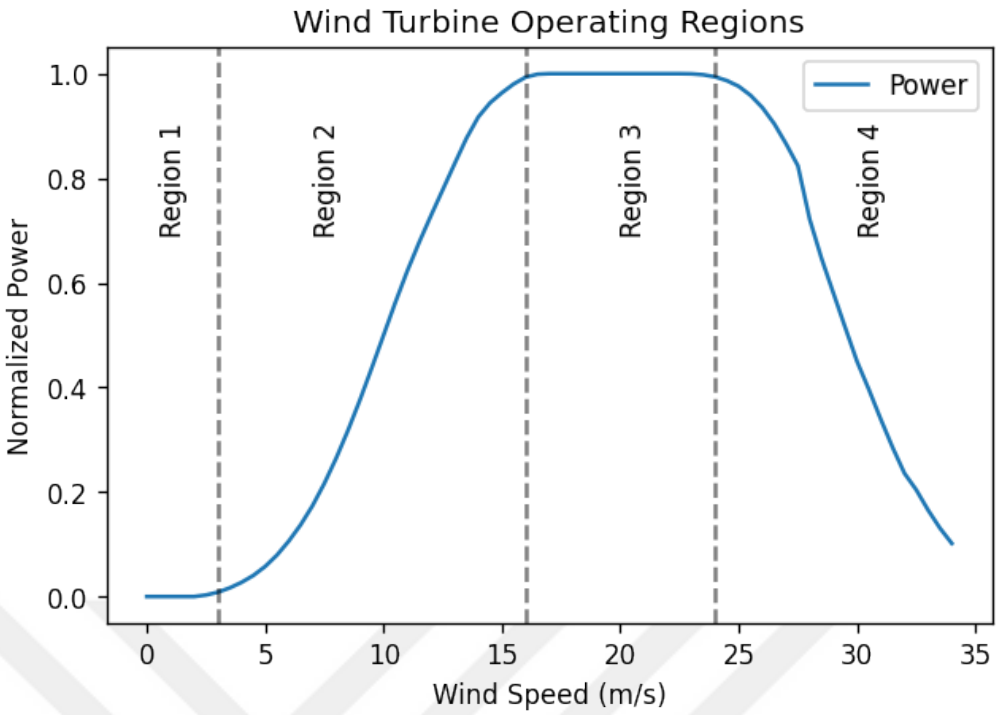

Figure 1.4: Power curve and operating regions.

capture the maximum amount of wind energy. The generated power is regulated by excitation current to match the specific set-point power curve.

- In region 3, the nominal power of the turbine is reached, and pitch angles are adjusted to keep the rotation speed at the nominal values.
- In region 4, the generated power is reduced by adjusting the pitch angles for structural health.

Power extraction, as described in Equation 1.1 is,

$$P = \frac{1}{2}\rho A_r u_{amb}^3 C_p(\lambda, \beta)$$

Where λ is the tip-speed ratio, and β is the pitch angle. Analytical approximations of C_p in terms of λ and β are discussed in [16], [17], and the tip-speed ratio is defined for the angular velocity ω of an R radius rotor,

$$\lambda = \frac{\omega R}{u_{amb}}$$

Then, power captured by a rotating body can be controlled by the tip-speed ratio and torque relation [18],

$$P = \omega\tau = \frac{\lambda u_{amb}}{R}\tau = \lambda u_{amb} T$$

1.3 Wind Turbine Wake Models

Wind farm production losses due to wake effects can reach up to 7-14% for offshore wind farms [19]–[21]. Onshore losses are estimated to be around 6% in [9]. Lundquist *et al.* (2019) estimated the wake losses due to commissioning a neighboring wind farm to Roscoe Wind Farm to be 5% on average and discussed the legal and commercial implications [22].

The earliest studies on modeling wind turbine wake are found by Lissaman (1977) [23], Faxen (1978) [24], and Lissaman (1979) [25], where the initial concepts around wind turbines wake and fluid interactions are discussed. With the increasing wind energy penetration, wake interactions became an issue that cannot be ignored. Wake losses occasionally deviate from the siting calculations [19]. This deviation drew attention to the need for better wake models[26]. Discussions around wind farm control for mitigating wake effects amplified the demand, especially for accurate analytical wake models. Desired models should be able to simulate wake interactions within a wind farm for each wind direction, wind speed, turbulence intensity, and yaw angle in a reasonable time while being able to capture the essential dynamics. CFD simulations and wind tunnel experiments are generally used to validate the analytical models; however computationally expensive for modeling and optimization of entire wind farms under the list of required atmospheric conditions.

1.3.1 NO Jensen Wake Model

Due to its simplicity and computational efficiency, the Jensen wake model [27] is generally the preferred model to illustrate wake effects. It can be easily applied and provides a good starting point for iterative and numerical models. It is derived from Equation 1.6 where $a = (1 - \sqrt{1 - C_t})/2$, Equation 1.3 and the momentum conservation. Model estimates a uniform velocity deficit of u_x at x distance from the rotor, where the wake is expanded to a diameter of $D + 2kx$ by,

$$\frac{u_x}{u_{amb}} = (1 - \sqrt{1 - C_t})(\frac{D}{D + 2kx})^2 \tag{1.8}$$

Where u_{amb} is the ambient velocity, C_t is the thrust coefficient of the wind turbine at u_{amb}, D is the rotor diameter, and k is the wake decay coefficient, defined empirically as half of the turbulence intensity.

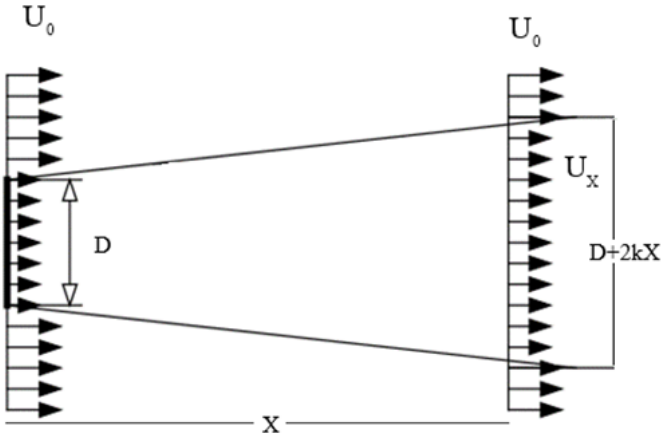

Figure 1.5: NO Jensen wake model, adapted from [27]

Commercial site assessment tool WAsP uses the Jensen Wake model [28]. The partial wake effect is commonly used in WAsP [28] as

$$\frac{u_x}{u_{amb}} = (1 - \sqrt{1 - C_t})(\frac{D}{D + 2kx})^2(\frac{A_{overlap}}{A_D}) \tag{1.9}$$

Where $A_{overlap}$ is the overlapping area of the expanded wake and the downwind turbine rotor area A_D.

1.3.2 Ainslie Wake Model

Ainslie (1988) Model assumes the wake to be a Gaussian distribution with 0 mean and a standard deviation of b. A simpler Gaussian distribution of wake deficit has been previously suggested by [30]; however, the Ainslie model incorporates turbulence intensity (TI) and empirical center-line velocity deficit D_m as,

$$D_m = \frac{u_{amb} - u_{r=0}}{u_{amb}} = C_t - 0.05 - ((16C_t - 0.5)TI/10)$$

A gaussian velocity deficit function can be written as,

$$\frac{u_{amb} - u_r}{u_{amb}} = D_m exp(-(r^2/2\sigma^2)) \tag{1.10}$$

Velocity deficit distribution around the center-line r distance from the center is described by Ainslie (1988) as,

$$\frac{u_{amb} - u_r}{u_{amb}} = D_m exp(-(\frac{\sqrt{3.56}r}{b})^2)$$

the standard deviation of the gaussian function or in the context of the wake model, the wake width b is derived as,

$$b = \sqrt{\frac{3.56C_t}{8D_m(1 - 0.5D_m)}}D$$

where r is the distance from the center of the rotor, D is the rotor diameter, and D_m is the initial velocity deficit at $r = 0$.

1.3.3 Gaussian Wake Models

Bastankhah and Porté-Agel (2014) [31] proposed an analytical wake model. Velocity deficit is considered in a Gaussian distribution shape, validated against LES simulations and wind tunnel experiments from previous research. The resulting model is straightforward and requires a single parameter, wake expansion coefficient k. Abkar and Porté-Agel (2015) [32] investigated the effect of atmospheric stability term on turbine wake. It is shown that stability greatly influences wake distribution with changes in the velocity deficit for both standard deviation and the mean. As expected, increased turbulence due to an unstable atmosphere refills the wake faster.

The deficit of wind speed is represented as a gaussian function,

$$\frac{u_{amb} - u_r}{u_{amb}} = Cexp(-r^2/2\sigma^2) \tag{1.11}$$

Inserting 1.11 into the thrust equation 1.1, where centerline velocity deficit C is defined as

$$C = 1 - \sqrt{1 - \frac{C_T}{8(\sigma/D)^2}} \tag{1.12}$$

using linear expansion of the wake in the x direction, as defined in [27],

$$\sigma = k^* x + \epsilon D \tag{1.13}$$

then the velocity deficit at hub height z_h is derived for lateral direction y and vertical direction z as,

$$\frac{u_{amb} - u_r}{u_{amb}} = (1 - \sqrt{1 - \frac{C_T}{8(\sigma/D)^2}})exp(-\frac{(z - z_h)^2 + y^2}{2(\sigma)^2}) \tag{1.14}$$

1.3.4 Wake Behind Yaw Offset Conditions

Kragh and Hansen (2014) showed that intentional yaw misalignment could reduce loads due to wind shear, using HAWC2 aeroelastic code simulations [33]. Optimum yaw offset angles are calculated to minimize the load variations up to 70% in low turbulence situations without production loss over nominal capacity. More on the investigation of damage equivalent loads can be found in [34], which assesses the loads due to yaw misalignment using OpenFAST aeroelastic code and field data in detail. Bastankhah and Porté-Agel (2016) reported a wake behind a yawed turbine to form a bean shape in wind tunnel experiments. However, this effect was not observed in LIDAR measurement on a commercial wind turbine in the study by Brugger *et al.* (2020) [36].

Observations from yaw misaligned wind turbines showed that the shape of the wake changes with yaw offset. The tilted shape of the wake can no longer be represented in a gaussian shape due to its asymmetry. Jiménez *et al.* (2010) showed an analytical relation for the wake trajectory due to yaw misalignment in [7] using LES simulations. Martínez-Tossas *et al.* (2019) [37] described the wake behind a yawed turbine as curled shape. Martinez-Tossas et al. solved the Navier-Stokes momentum equation with the vorticity equation to represent wake shape with the elliptical distribution. The wake of a yaw misaligned wind turbine appears as 'curled' in addition to being deflected. An efficient wake model for yawed wind turbines is introduced. The wake model is generated from the linearized RANS momentum equation, using assumptions for wake rotation, vertical wind profile, turbulent viscosity, and boundary conditions. Curled wake model is validated against LES simulations using the SOWFA solver. For two-turbine settings, the curled model agrees with the LES simulation; however, it overestimates the gain for three-turbine settings. The proposed model is computationally efficient and can be used for wake steering and real-time wind farm control.

1.3.5 Cumulative Curl Model

The gaussian curled hybrid model by Martínez-Tossas *et al.* adds the curled wake effect for yawed conditions to the gaussian wake model. Limitations of the previous models, including the gaussian curled hybrid, are highlighted by Gunn *et al.* [38] and Doekemeijer *et al.* [39]. Both studies showed wake combination lacking, especially for large series of wind turbines. Wake superposition of deeper arrays of wind turbines is improved by Bay *et al.* (2022), implementing the model combined wake effects from Bastankhah *et al.* instead of linear or root sum square superposition methods.

The cumulative curl model by Bay *et al.* (2022) is built upon Bastankhah *et al.* (2021) [41] with the additions from Blondel and Cathelain (2020) [42], which uses a higher-order Gaussian wake model to represent the shape of the wake. The order of the Gaussian function is empirically derived and calibrated from wind tunnel experiments, LES simulations, and field measurements, and near-wake corrections are implemented from Qian and Ishihara. Wake steering application heavily depends on the accurate modeling of a yawed wind turbine. The addition of the curled model is implemented from [37]. The cumulative curl model uses near-wake improvements from [42] and offers vectorized structure, significantly improving computation times [40]. Wake deficit is defined as an m-th order gaussian distribution [42] as,

$$\frac{u_{amb} - u_r}{u_{amb}} = C_n exp(-r^m/2\sigma^2) \tag{1.15}$$

The centerline (maximum) velocity deficit of the current turbine is derived by integrating the thrust force on the wind as,

$$C_n = C_k(a_m - \sqrt{a_m^2 - \frac{mC_{t,n}cos(\gamma_n)}{16\Gamma(2/m)\sigma_n^{4/m}C_k^2}}) \tag{1.16}$$

Γ is the gamma function is the result of the integration, γ_n is the yaw angle of the current turbine, $C_{t,n}$ is the thrust coefficient, and C_k is defined to accommodate for the wake combinations into the centerline velocity deficit from upwind turbines, C_i and the

contribution of wake upwind turbines are represented by λ_{ni}

$$C_k = 1 - \sum_{i=1}^{n-1} \lambda_{ni} \frac{C_i}{u_{amb}} \tag{1.17}$$

Order of the gaussian distribution is found by curve fitting in [42] as,

$$m = a_f exp(b_f \tilde{x}) + c_f \tag{1.18}$$

$a_f = 3.11, b_f = -0.68, c_f = 2.41$ as constant from the work of [42].

a_m is used to simplify the equation 1.16,

$$a_m = 2^{2/m-1} \tag{1.19}$$

Wake contribution from previous turbines i on the turbine n is defined in [41], are defined as,

$$\lambda_{ni} = \frac{\sigma_n^2}{\sigma_n^2 + \sigma_i^2} exp(-\frac{(y_n - y_i - \delta_y)^2}{2(\sigma_n^2 + \sigma_i^2)}) exp(-\frac{(z_n - z_i)^2}{2(\sigma_n^2 + \sigma_i^2)}) \tag{1.20}$$

Similar to the expression in Equation 1.13, the standard deviation is expressed, normalized with rotor diameter D,

$$\sigma_n = k\tilde{x} + \epsilon \tag{1.21}$$

Wake expansion coefficient k is defined in terms of

$$k = a_s TI + b_s \tag{1.22}$$

$$\tilde{x} = \frac{|x - x_n|}{D} \tag{1.23}$$

$$\epsilon = (c_{s1} C_{t,n} + c_{s2}) \sqrt{\beta} \tag{1.24}$$

$$\beta = \frac{1 + \sqrt{1 - C_{t,n}}}{2\sqrt{1 - C_{t,n}}} \tag{1.25}$$

1.3.6 Additional Effects

Power law for the wind shear is used to calculate effective wind speed at the rotor plane in the simulations using [14],

$$u(z) = u(z_{hh})(\frac{z}{z_{hh}})^{\alpha} \tag{1.26}$$

where $_{hh}$ subscript denotes the hub height. Shear exponent $\alpha = 0.18$ is used from year-long measurements at the nearby met-mast [44].

To compare the manufacturer's power curve and the measured power curve, air density normalization in IEC standard 61400-12-1 [13] is used by changing the wind speeds corresponding to the power on the power curve. Specifically for "wind turbine with active power control" for yearly average air density as,

$$u_{site} = u_{norm}(\frac{\rho_0}{\rho_{site}})^{1/3} \tag{1.27}$$

where u_{norm} is the wind speed given by the manufacturer power curve, ρ_0 is the standard air density of 1.225 kg/m^3 and ρ_{site} is the yearly average air density of 1.19 kg/m^3 measured at the site [44].

Wind veer effects observed at the nearby met-mast are in the order of 1^o direction changes throughout the rotor plane[44]; thus wind veer effects are not integrated for this study.

1.4 Wind Farm Control

This section defines wind farm control as the collective control of the wind turbine units to achieve maximum overall wind farm production. Two schemes are relevant for wind farm flow control. The first one is Axial induction control, sometimes named in the literature as; de-rating. Second is the wake steering approach, otherwise named in the literature as; wake redirection, wake deflection, yaw misalignment, and yaw control.

1.4.1 Axial Induction Control

As described in equation 1.3, axial induction relates to the decrease in wind velocity past the rotor plane. Static axial induction control has been used by down-rating the upwind turbine. In the literature, axial induction control is controlled by pitch angle β, yaw angles γ, tip-speed ratio λ, or rotational speed ω. All mentioned control inputs correspond to changing the power set-point, although wake mixing effects are also exploited by dynamic β and λ control.

Initial research mainly focused on static axial induction. The earliest example of wind farm control for aerodynamic interactions is found in Steinbuch *et al.* (1988) [5] controlling the tip-speed ratio; it is shown in a simulation that increasing total production is possible by down-rating upwind turbines. Wind tunnel study by Bartl and Sætran (2016) [6] used a range of λ and β to measure performance gain in a two-turbine-array scaled wind farm model. The author found no net gain in the experiment λ control, although loads on each turbine were evened out. β control however reduced the array output. Dilip and Porté-Agel (2017) [45] run LES simulations for two-turbine-array wind turbines for a range of β control inputs. Improvements of 0.5% to 2.8% were noted depending on spacing and turbulence intensity for stall pitch angles (negative pitch values), whereas feather pitch angles worsened the overall production.

Dynamic induction control variants were also used to introduce periodic induction

change, taking advantage of wake mixing. Frederik *et al.* (2020) [46] used periodic individual pitch angle variations of 1 deg/s to induce mixing in the wake. The experiment is executed in SOWFA LES code. Results are compared to dynamic induction control by collective pitch control, yaw control, and static induction, reporting a 6% increase in the wake stream tube. Gebraad and Wingerden (2015) [47] designed a controller for maximum power-point tracking for Princess Amelia Wind Farm, with control input as axial induction factor a. Using gradient-based optimization in the SimWindFarm controller toolbox, a 4% effective gain is reported.

Initial field experiments for axial induction control through pitch control are conducted by Schepers and Pijl (2007) [48] where results from research wind farm EWTW are documented. Overall production gain is limited to <0.5%; however, a decrease in fatigue loads and noise is also reported. Continued experimentation in EWTW Boorsma (2012) found power gain inconclusive.

Axial induction control using pitch control is applied to Goole Wind Farm by [50] in a 12-month-long field experiment. Optimal pitch angles are calculated based on FarmFlow, a parabolized CFD tool. A 1x5 wind turbine row was used for the study, where the controller toggled on and off every 3.5 days to create a control group. A 3.5 % production increase in the wake sector is observed, corresponding to a 0.37% increase in AEP.

Another field experiment using axial induction control is the work by Bossanyi and Ruisi (2021) [51], implementing a controller for the nine turbines of Sedini Wind Farm. A controller is designed to reduce the power set-points of wind turbines optimally. Wind farm measurements are used to find the best choice of wake model and its parameters. LongSim code is used for analytical modeling and optimization for different atmospheric conditions. The axial induction controller is turned on and off every 35 minutes to provide a control group. Data collected over six months showed a 1.7% to 2.4% increase in average power compared to similar wind conditions when the induction controller was toggled off. An ongoing experiment by Bossanyi *et al.* (2022) for axial induction control is available in [52] where the controller design for the study is published.

Another use case of axial induction is proposed by Eguinoa *et al.* (2021) [53] as an integration of wind farm control for providing balancing market and ancillary services (reserve capacity) to the grid. This heavily relies on accurate measurements of available

power [54], control solutions for tracking desired power set-points, and farm modeling for all atmospheric conditions.

1.4.2 Wake Steering

Wind turbine yaw misalignment effects are initially investigated for performance power analysis. Wind tunnel and field experiments [55]–[57] showed that yaw misalignment resulted in skewed wake trajectory, and a decrease in axial induction is reported. Deflection in the wake trajectory is later investigated by Jiménez *et al.* (2010) [7] to mitigate the wake effects using an LES model, which was in good agreement with the compared wind tunnel experiments.

The wake of a yaw misaligned wind turbine appears as 'curled,' in addition to being deflected. An efficient wake model for yawed wind turbines is introduced by Martínez-Tossas *et al.* (2019) in [37]. The wake model is generated from a linearized RANS momentum equation, including the effects from wake rotation, vertical wind profile, turbulent viscosity, and boundary conditions. Curled wake model is validated against LES simulations using the SOWFA solver. For two-turbine settings, the curled model agrees with the LES simulation; however, it overestimates the gain for three-turbine settings. The proposed model is computationally efficient and can be used for real-time wake steering and wind farm control. This model is commonly used in [12] as the GCH model.

King *et al.* (2021) [58] used a hybrid wake steering model, modifying the Gaussian wake model Bastankhah and Porté-Agel (2014) [31] with curl model Martínez-Tossas *et al.* (2019) [37], with the addition of effects of secondary steering is proposed. Counter-rotating vortices [59] due to yaw steering add additional wake recovery effects downwind, even if the downwind turbines are not steered, which is called secondary steering effects. The model is validated using high-fidelity SOWFA-LES simulations using 3, 5, and circular 38 turbine settings for high and low turbulence conditions. The hybrid model outperforms the Bastankhah model; however, it mildly overestimates the power gains compared to LES. This work is implemented in [12] as an addition to the GCH model, available as secondary steering.

Initial yaw steering field experiments are conducted by Wagenaar *et al.* (2012) using small-scale wind turbines in the Energy Research Center of Netherlands' scaled wind farm. There was no conclusive evidence of the effects of wake steering in the downwind turbines.

A field study of wake steering in an offshore wind farm in China is carried out by Fleming *et al.* (2017) [61] by controlling a single wind turbine upwind and measuring the effects on three downwind turbines. An additional wind turbine is used as a reference to measure the impact of wake steering. The experiment was run for four months to collect 20 Hz SCADA measurements and another four months after wake steering was activated. The power increase in the maximal wake direction is observed to be less than the simulated. The seasonal effect made the comparison difficult due to the selection of the control period as four months before the actual wake steering implementation.

Fleming *et al.* (2019) [8] continued field experiments for wake steering with the takeaways from the previous investigation as toggling the controller on and off periodically to use as a control group. Initial results are reported, including the first eight months of the wake steering study. FLORIS optimization tool [12] with Gaussian model is used to find the optimal yaw angles for two yaw-modified controlled turbines and a downstream turbine. Simulated optimum yaw angles are integrated as a lookup table for controlled turbines with wind speed and direction as variables. The wind vane signals of the controlled turbines are modified by the lookup table and then fed to the yaw actuator with a modified offset. The modified signal is toggled every hour to compare the wake steering and the default case. Three months of data is collected, and wake steering gain is calculated when the modified controller has been off. 14% energy is recovered through wake steering in the downwind turbine, and a 4% increase in energy is observed considering losses due to upwind intentional yaw misalignment. Compared to the similar FLORIS results of a 4.1% energy increase, wake steering models show potential for yaw controller design.

Fleming *et al.* (2020) [9] continued the field experiments for the wake steering campaign [8], the second phase of the study was conducted for ten months with lessons learned from the first phase. Wake experiments are completed on two controlled and one downstream turbine under wake. A lidar, two sodars, and a met mast measured atmospheric conditions. Different Gaussian wake models are investigated for the predictivity of wake steering gains. Modification to the controller is toggled on and off every hour to validate

yaw steering effects. A 6.5% reduction in wake losses is observed, nearly half of what was predicted from FLORIS models. Moreover, there were losses from unintended yawing due to the default yawing actuator. A more robust optimal look-up table is recommended for future studies to improve unintended yawing conditions. Additionally, a standalone yaw-offset controller is recommended instead of modifying the wind vane input to remedy unintended yawing.

Another field experiment is conducted by Howland *et al.* (2019) for six wind turbines in a single row located in Alberta [62]. 7% increase in power production is measured for complete alignment in a 10-day-long field study. Author more recently released the results from an experiment in a wind farm located in India, conducted on three wind turbines [63]. For the wake sector in Region 2, production increase is recorded at around 3%, and overall improvement in the wake sector is 1.2%. AEP improvement is estimated to be 0.3% for all wind speeds and directions.

More field experiments are available from Annoni *et al.* (2018) in [64], Doekemeijer *et al.* (2021) in [65], Simley *et al.* (2021) in [66].

CHAPTER 2

METHODOLOGY

The main objective of this study is to assess the maximum production achievable at a wind farm in wake effect by controlling the wake trajectory through wake steering. This chapter focuses on utilizing operational wind farm data for wake steering assessment and simulating the wind farm to find optimal yaw offset angles for wake steering application.

2.1 Site and Plant Description

The wind power plant is located on a peninsula in İzmir, Turkey. 5 wind turbines are commissioned on a hilltop 460m above mean sea level (AMSL) with a total nameplate capacity of 15 MWm. Wind turbines are variable-speed, pitch-regulated, direct-drive with low-speed synchronous annular generators. A village to the west is located 1.9 km away, 160m AMSL and another is to the east, 2.6 km away, 60m AMSL. There is an additional wind farm 3 km to the south. Figure 2.1 shows the contour of the nearby terrain and the slope map. Wind turbines are not entirely aligned due to topography and have an average spacing of 2.82 ± 0.06 rotor diameters.

The wind farm is surrounded by complex terrain due to year-long vegetation and sloped elevation. The wind rose from the site with 5^o wind direction bins is available in 2.2a. The dominant wind direction is north for all seasons. The site is analyzed in terms of 4 main sectors due to wake losses, denoted north (N), east-south-east (ESE), south (S), and west-north-west (WNW). The distribution of winds for each sector is shown in Figure 2.2b. Wind turbines, often denoted as WT1 to WT5, are placed from ESE to WNW direction, where WT5 is the west-most turbine.

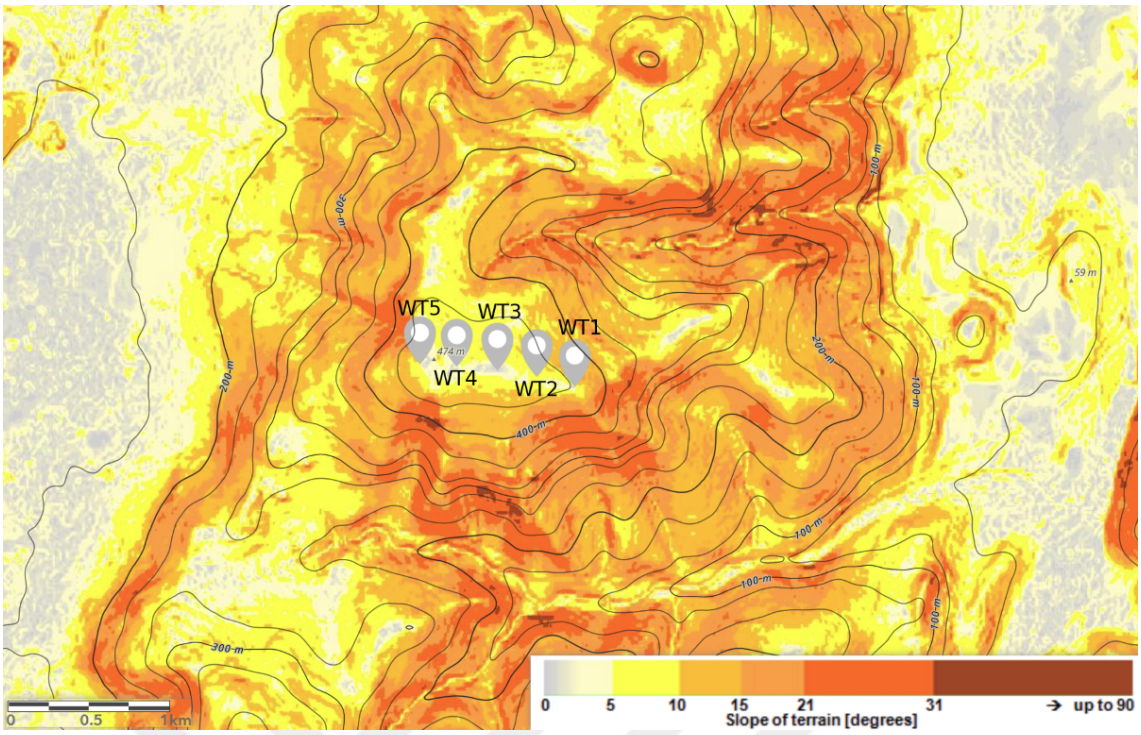

Figure 2.1: Terrain slope map of the site [67]. Wind turbines are on the five placemarks.

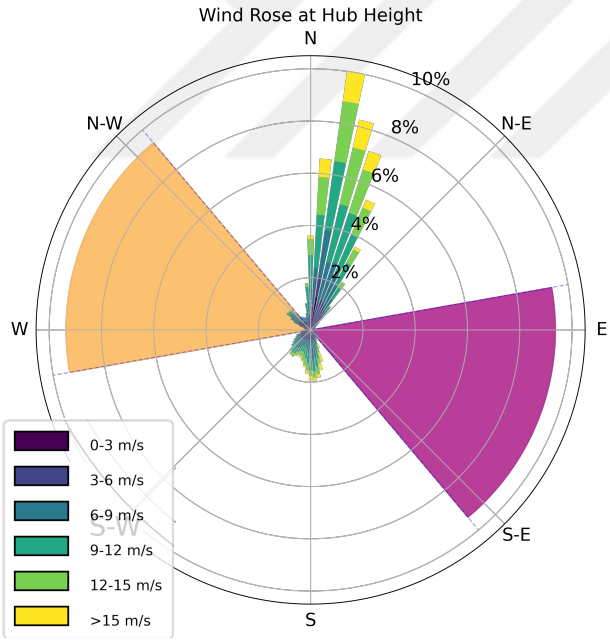

(a) The wind rose at the site.

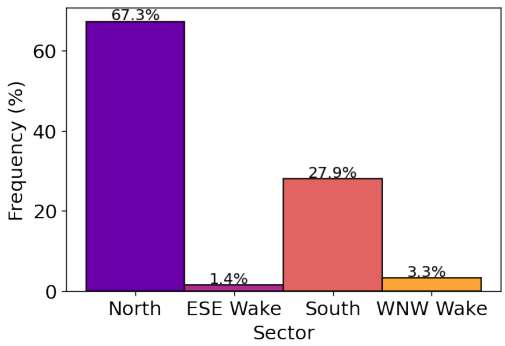

(b) Distribution of wind frequency per sector for wind speeds greater than 3m/s.

Figure 2.2: Distribution of wind across directions. Purple (ESE) and orange (WNW) tilted regions show the sectors where any turbine is under the wake effect.

2.2 Operational Data Analysis

5-year-long operational wind farm data for five wind farm turbines was acquired for the study. Data consists of time series with 10-minute spaced intervals for each wind

turbine. Most variables are the mean value recorded in 10 minutes and the minimum and maximum values recorded in that period. A complete list of recorded SCADA measurements is available in Table 2.1.

Table 2.1: Available operational data in 10-minute intervals.

Variable	Unit	Symbol	Resolution	
Wind speed	m/s	u	0.1 m/s	Atmospheric conditions
Temperature	^oC	T	1^o	
Precipitation	mm/min	-	1 mm/min	
Visibility	km	-	1 m	
Ice amplitude	%	-	1%	
Power	kW	P	1kW	Operational variables
Reactive power	kVAR	R	1kVAR	
Rotation speed	rpm	ω_{rpm}	0.01 rpm	
Energy	kWh	E	1kWh	
Turbine availability	kW	P_{avail}	1kW	
Operation time	h	-	1 min	
Yaw angle	^{o}	γ	1^o	
Pitch angle	^{o}	β	0.1^o	
Status Codes	-	-	1 s	

Wind speed, measured from the nacelle-mounted anemometer, records the mean, maximum and minimum measurements in 10-minute periods. Nacelle-mounted anemometers are calibrated with nacelle transfer function (NTF), as described in IEC manual 61400-12-2, to mitigate the effect of turbine structure on the measurements [68]. This data is not reliable under wake conditions since and method described in Section 2.2.4 is used to measure wind speeds under wake conditions.

Absolute wind direction is generally not measured by nacelle-mounted wind vanes. The wind vane measures relative offset from the current wind direction, and the yaw position is adjusted accordingly. Wind direction is acquired from corrected yaw positions, as described in Section 2.2.2.

Power values are the main subject of this study and are discussed in detail in Section 2.2.3 and Section 2.2.4. Turbine availability is used to determine the wind turbines' state and current set-point. A list of availability columns are:

- Available power in the wind: Theoretical power available in the wind, regardless of

technical problems, limitations, or external set-points.

- Available power limitation due to technical limitations: Maximum power available when technical limitations such as overtemperature and converter faults are detected.
- Available power limitation due to external forces: Maximum power available after a storm or grid fault is detected.
- Available power limitation due to external set-point: Maximum power available when a set-point is activated, e.g., transmission system operator.

If available theoretical power is under any limitations mentioned above, the "curtailed" flag is set, and flagged intervals are excluded from any performance-related assessment. External set-points are easily recognizable from the Figure 2.3 where transmission system or farm operator set-points limit the operation. Additionally, when the turbines are not operational, samples are shown to be clumped on a line at zero power.

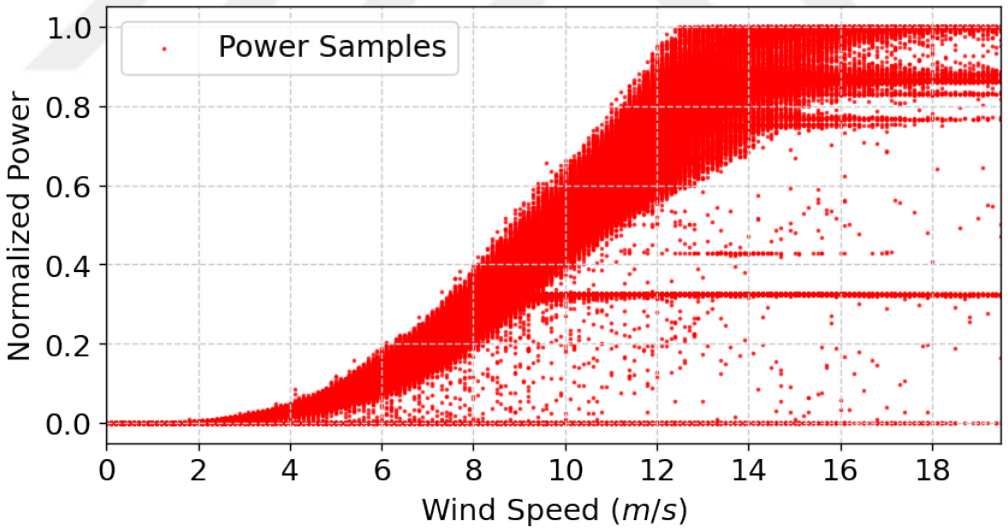

Figure 2.3: Raw wind speed vs. power data.

Operational status codes are asynchronous logs, recording the events in the individual turbines at exact timestamps and duration of the status. Most messages are due to a turbine starting operation after cut-in speed is reached or operational after a technical limitation, e.g., maintenance, yawing cable untwist, overtemperature, etc. Status messages are initially converted into a 10-minute format. Later messages are aggregated

if multiple status messages appear in the same 10-minute period. Message duration and the number of error occurrences are also aggregated similarly. Finally, empty messages in the time series are forward-filled to reflect the last status message to the 10-minute wind turbine data. This works since any status message is followed by a "turbine operational" message whenever the issue is resolved. Status messages are used to assign the "operational" flag, and flagged data is excluded from power performance-related analysis.

Using available variables, categorical labels are assigned time stamps to reflect operational status. A list of derivational data is available in Table 2.2. The subsequent sections explain the derivation of wind direction, power curve, reference wind speed, and power.

Table 2.2: Derivational data.

Derivational Data	Type/Unit	Related Data
Operational	Boolean	Status codes, operation time
All-Operational	Boolean	Operational
Curtailment	Boolean	Availability
Any-Curtailment	Boolean	Curtailment
Under wake	Boolean	Wind direction
Sector	Categorical	Wind direction
Limiting factor	Categorical	Availability
Wind direction	^{o}	Yaw angle
Tip-speed ratio	-	Rotation speed, wind speed
Reference wind speed	m/s	Wind Speed, sector
Reference power	kW	Operational flags, reference wind speed
Measured power curve	-	Operational flags, wind speed

2.2.1 Data Filtering

Acquired data was raw and subjected to localization or other settings in the logging computer and could not be used as is. For example, all power or energy-related columns used "dot character" as the thousands separator while others used it as the decimal delimiter. Initial data cleaning removes implausible values like negative wind speeds, repeating

timestamps, timestamps recorded outside 10-min intervals, NaN values, max values lower than min or mean values and corrupted values like repeating implausible values in multiple columns. Plausible negative power production values are set to zero, indicating the generator's initial excitation. Periods of maintenance or turbine malfunction are also filtered using observation and recorded operational status codes. The remaining data is fully conserved, and flags and categories are assigned depending on different use cases as listed in Table 2.2.

2.2.2 Wind Direction Correction

Most SCADA systems do not record wind vane measurements, which only record the relative distance of the nacelle from the mean wind direction. The yaw position is not calibrated as opposed to the wind vane, and the measured position is generally offset by a constant amount. This is due to the nacelle-mounted wind vane reporting the relative wind direction, not the actual direction [68]. A re-calibration process, similar to [69]–[71], is used to correct the wind direction values.

Wind Turbine 3 (WT3) is used as the reference, which showed the best agreement with the median wind direction from the site measurements. Measurement calibration is performed for the open sectors north and south. Constant wind direction disagreements follow a Gaussian distribution after shifting all directions by 180^o in Figure 2.4. A Gaussian fit is used, and the mean of the Gaussian function is used to calibrate each wind turbine's yaw angle. The list of applied corrections is available in Table 2.3. All wind turbine equipment is reportedly calibrated periodically during maintenance following the standard [68]. The complete set of wind roses for each wind turbine, before and after the calibration, is available in Figure B.3.

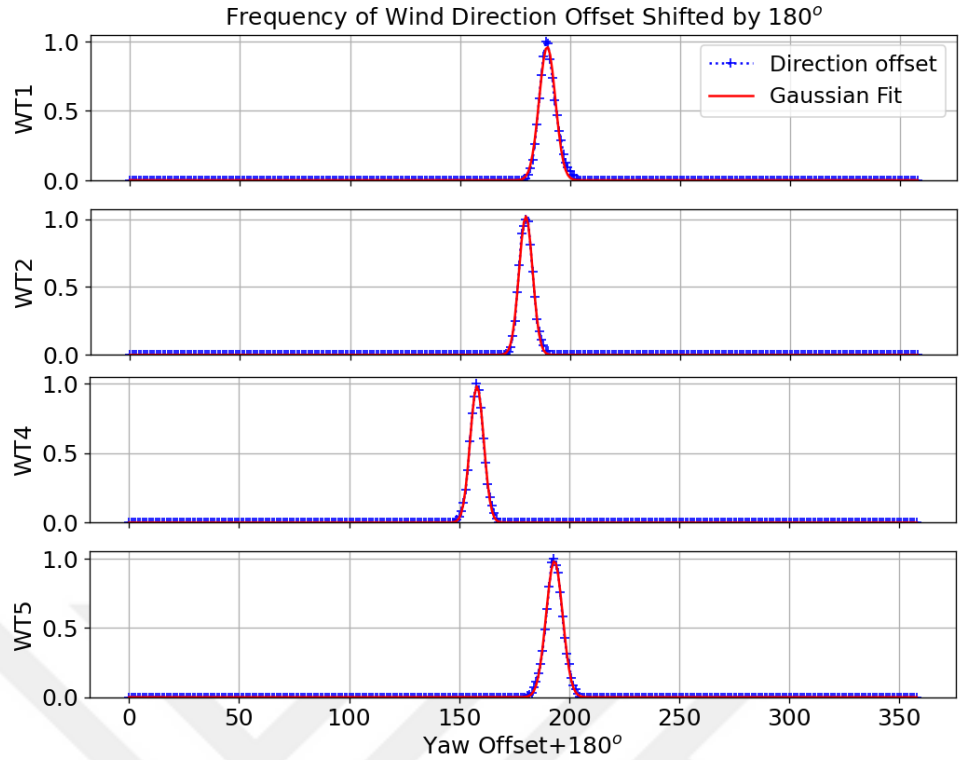

Figure 2.4: Wind direction calibration from yaw angles. Only samples from the north and south sectors are used, and Plant 3 is used as a reference.

Table 2.3: Correction offset for each turbine and the uncertainty due to correction. WT3 is used as the reference.

Plant	Mean Offset (^{o})	Std.Dev. (^{o})
WT1	-9.7	3.7
WT2	+0.1	3.0
WT4	+21.9	3.1
WT5	-13.3	3.7

2.2.3 Site Specific Power Curve Estimation

The power performance of a wind turbine is measured on a test site as its power response to different wind speeds, which is then normalized to generic atmospheric conditions. Local climate and topography can change the power curve significantly. In the IEC standards for wind turbine power performance measurements [13], essential factors for determining the power curve are given as air density, wind shear, wind veer, atmospheric stability, and the nearby topography. Manufacturer-published wind turbine

power curves may not be up-to-date or, more commonly, do not represent the turbine response in site-specific conditions. Additional upgrades and blade add-ons also improve the performance and, thus, the power curve. Wind turbines at a site may also be certified to improve the nominal capacity of the generators, as long as site and equipment requirements are met [72]. Conversion to a site-specific power curve is available through site assessment software, following IEC standard [14] and with more detail in [13].

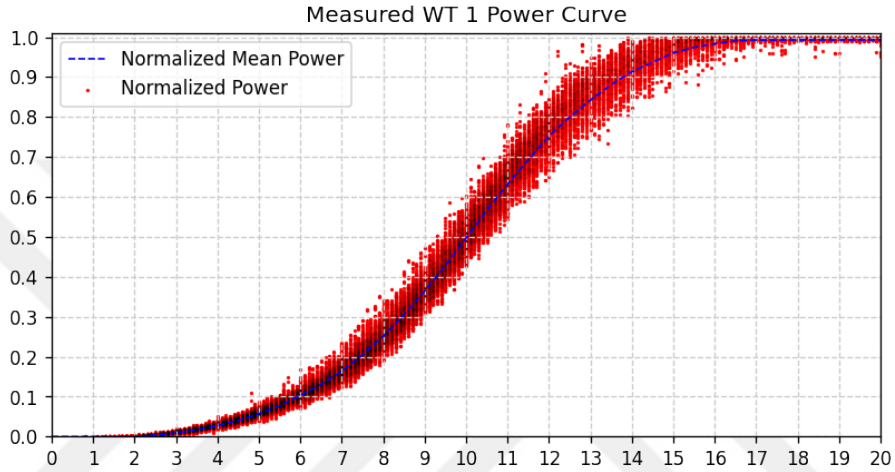

Figure 2.5: Scatter plot of WT1 and measured mean power curve.

This study uses a deterministic approach to measure the site and turbine-specific power curves. Power curves are empirically generated using the flags and categories specified in Section 2.2 as; not under wake, north sector, operational, and not curtailed. Due to the electrical capacity set by the transmission system operator (TSO) before June 1st, 2022, the wind farm was curtailed to the 87% of the nominal capacity. This is verified by the supplied data and the recorded measurements from the national TSO, TEIAS, which is shared publically by EPIAS [73]. Power curve measurements for turbines 1-4 are straightforward and typically work with no limitations. However, turbine 5 has a set-point of 1/3th the nominal capacity, and measurements above the set-point took place during maintenance periods; a lightning incident in Jan 2019, where turbine 1 stopped production for four months. Measured power curves for the nominal set-point for all turbines show only slight variation with a Pearson correlation coefficient of 99.95%. Since the study aims for a streamlined process for wake steering assessment for any wind farm, power curves are set individually from empirically derived measurements, even if the variations

are indistinguishable. Since the power curves were indistinguishable on a plot, the average wind farm power curve is plotted in Figure 2.6.

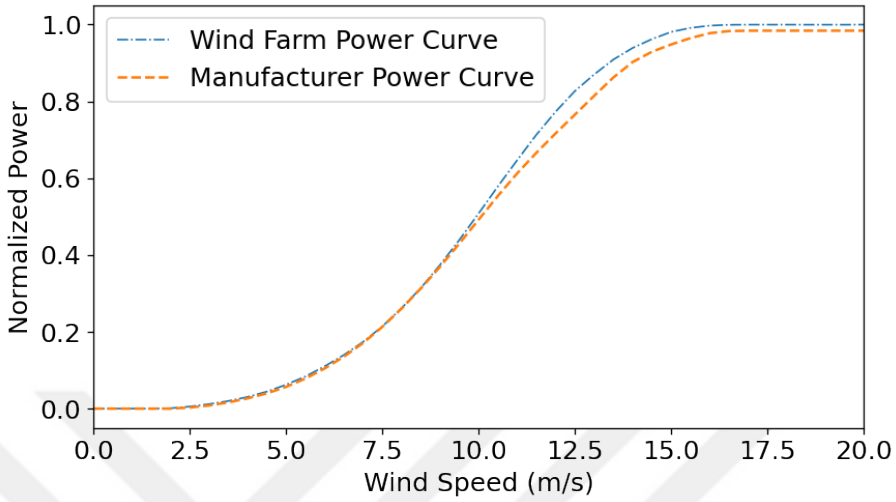

Figure 2.6: Measured and manufacturer-published power curve.

2.2.4 Reference Wind Speed and Reference Power

Wake effects are the most significant factor resulting in a power deficit for wind turbines operating at normal conditions, sited under the certifiable standards [14]. Reference values for wind speed and power are required to measure the wake effects. Reference wind speed is acquired differently for each wind sector defined in Fig. 2.2a. For undisturbed north and south sectors, mean wind speed measurements are used as references. The east-most wind turbine wind speed measurement is used as a reference for the ESE wake sector. Similarly, the reference wind speed from the WNW wake sector is used as the west-most wind speed measurement. Reference power is calculated by matching the reference wind speed at 0.1 m/s resolution to the power curve generated in Section 2.2.3 for each wind turbine individually.

2.2.5 Measured Wake Effects

Wake effects for the wind farm are calculated using the median ratio P/P_{ref} for each wind direction bin for different wind speeds. Derivation of P_{ref} is defined in Section 2.2.4 and P is the power value for each time stamp. Only valid samples are used by filtering the data using flags defined in Table 2.2. Samples with fully operational turbines that were not curtailed are used to measure wake effects. The resulting P/P_{ref} vs. Wind Direction is plotted in Figure 2.7. The uncertainty of each wind direction in a bin is displayed as boxplots where the box region indicates the interquartile range (IQR) between the 25th and 75th percentile. The lower whiskers indicate the 25th percentile - IQR and the upper whiskers the 75th percentile + IQR. The stacked line plot of wake losses in the WNW sector for each wind turbine is displayed in Figure 2.8. Observed wind frequency from the ESE sector is relatively low, which is also reflected in increased uncertainty on the P/P_{ref} box plots of Figure 2.7. Thus, only the WNW wake sector is considered for evaluating the wake model performance.

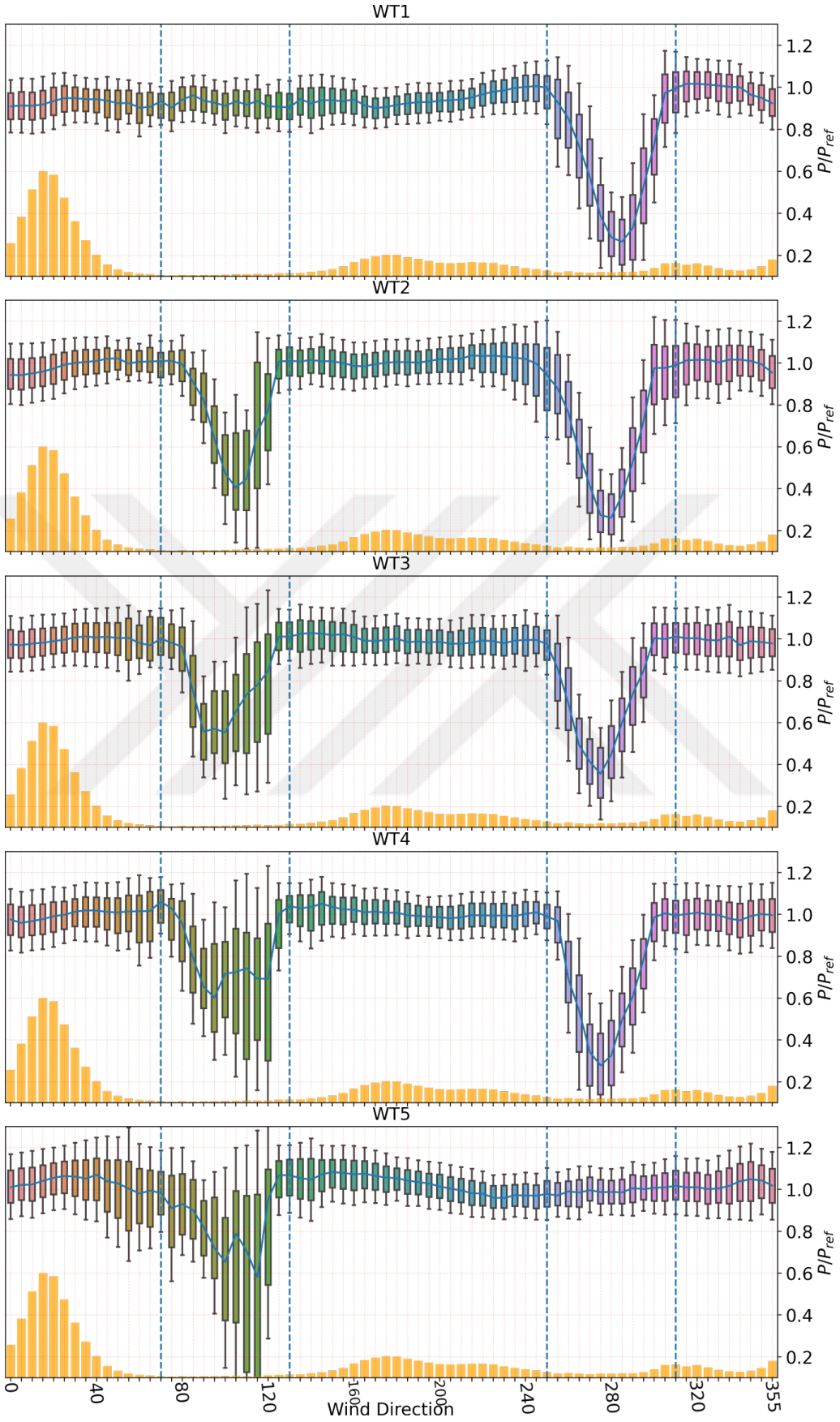

Figure 2.7: Measured wake losses and frequency of each wind direction bin for the wind farm at 9 ± 3 m/s wind speed.

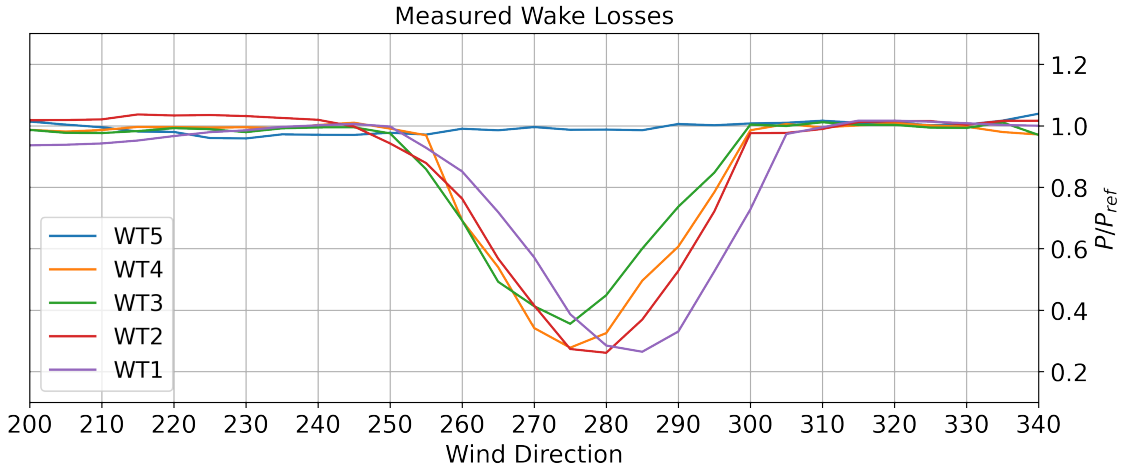

Figure 2.8: Line plot of wake losses for each turbine for WNW sector for 5^o wind direction bins at 9 ± 3 m/s wind speed .

2.3 Validation of the Acquired Data

TSO-recorded hourly meter data [73] is used to validate the operational data timestamp orientation and verify the recorded time zone. Observed deviation from operational and TSO data is mainly due to SCADA not recording transmission losses which are expected to be 0.5% to 2%. From Figure 2.9, the observed 0.5% bias is attributed to the transmission losses up to the point of interconnection. The refined power measurements after the consolidation process of the energy market are released in [74], however, records only go back until 2021, which is outside the time range of most of the SCADA measurements.

2.4 FLORIS Setup and Parameters

FLORIS is developed by NREL (2022) [12] to solve steady-state wake interactions in wind farms. The project has been in development since 2013 and has been validated in the literature using CFD simulations [37], [75], [76], wind tunnel [77]–[80] of wake models as well as wind farm field studies [8], [9], [65], [66]. The wake steering models are

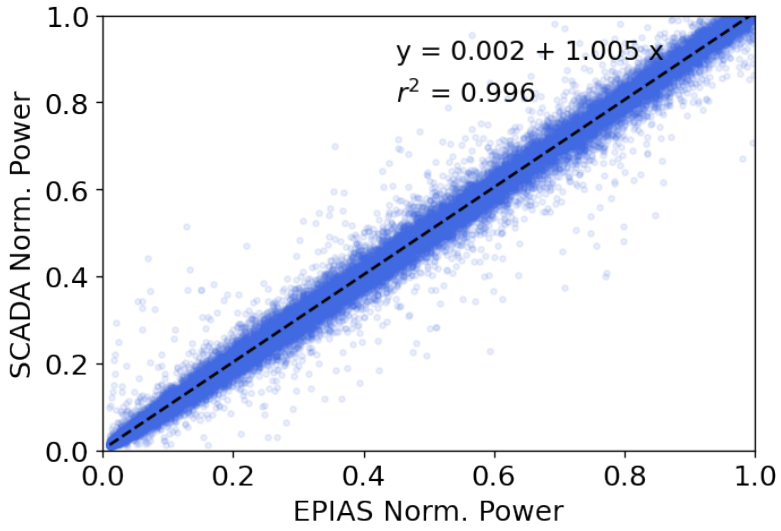

Figure 2.9: Comparison of power measurements and EPIAS recorded power generation at the site.

discussed in more detail in Section 1.4.2. FLORIS enables the use of analytical models for wind farm induction and wake steering simulations in a reasonable time for real-time control or digital twin calibration applications. Jensen's (Park) model in FLORIS uses the wake model defined in Section 1.3.1. The multizone wake model is based on the Jensen wake model [81], and Jimenez deflection model [7] for wake steering and as suggested in [75], [82]. The Multizone model defines and calibrates the wake for three zones, near-wake, far-wake, and mixing zone individually. The TurboPark model [83] uses a modified Jensen (Park) wake model. It introduces a gaussian wind speed deficit as defined in [31] on the wake expansion model of the Jensen model. FLORIS also offers gaussian curl hybrid and cumulative curl models described in Sections 1.3.3 and 1.3.5, which are the focal points of this study.

FLORIS is configured for the farm layout; each wind turbine is configured individually, and empirically derived power curves are set. Since FLORIS uses C_p values for the simulation, C_p is calculated scaling the manufacturer $C_{p_{OEM}}$ by $p_{OEM}/p_{measured}$ for each wind speed bin. Figure 2.10 shows the summary of the procedure implemented to FLORIS interface.

The AEP of the wind farm is estimated for no-wake, with-wake, and wake steering calculations using the frequency of each wind speed and wind direction from 5-year-long site data. Two gaussian curl models are used, and the best-performing wake model is used to calculate the wake steering assessment. Both the gaussian curl hybrid (GCH)

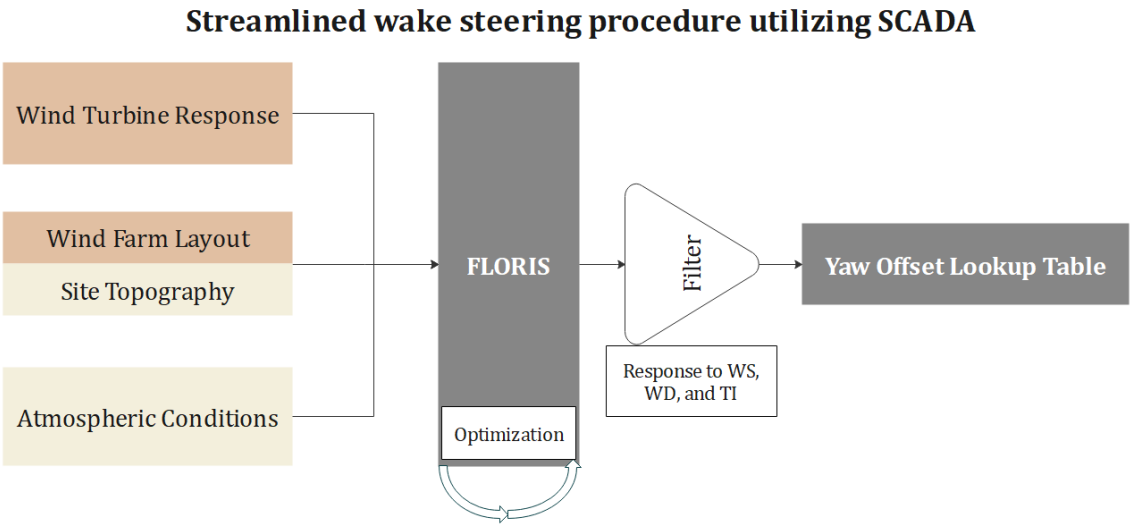

Figure 2.10: Summarized procedure for utilizing operational farm data for wake steering assessment and application.

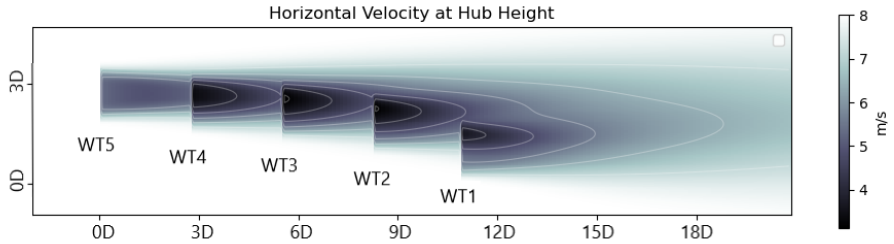

(a) Horizontal velocity profile at hub height.

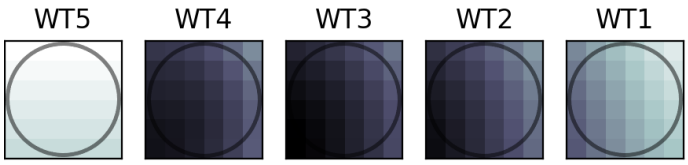

(b) Rotor cross-section.

Figure 2.11: Velocity profiles at 8 m/s ambient wind speed and 270^o wind direction.

and cumulative curl (CC) model estimates the effects of the counter-rotating vortices to better predict yawed conditions. The Jensen wake model is not considered due to the discontinuity of the top-hat shape and the resulting loss of resolution in partial wake situations. Considering Figure 2.12, the GCH model overpredicts the wake losses for the first downwind turbine and underpredicts the wake losses for the latter turbines in the array. CC model is better at representing the wake effects deeper down the array and errors are consistent with the selection of the upwind turbine as the reference.

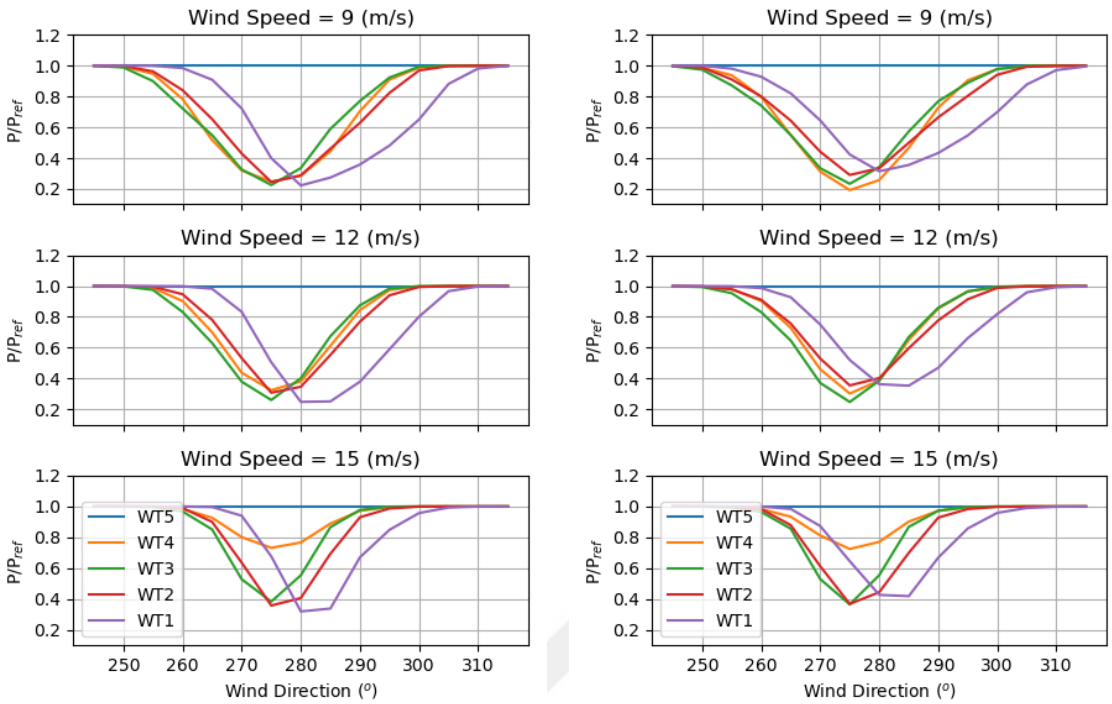

(a) Cumulative curl model. (b) Gaussian hybrid curl model.

Figure 2.12: Simulated wake losses for WNW sector winds.

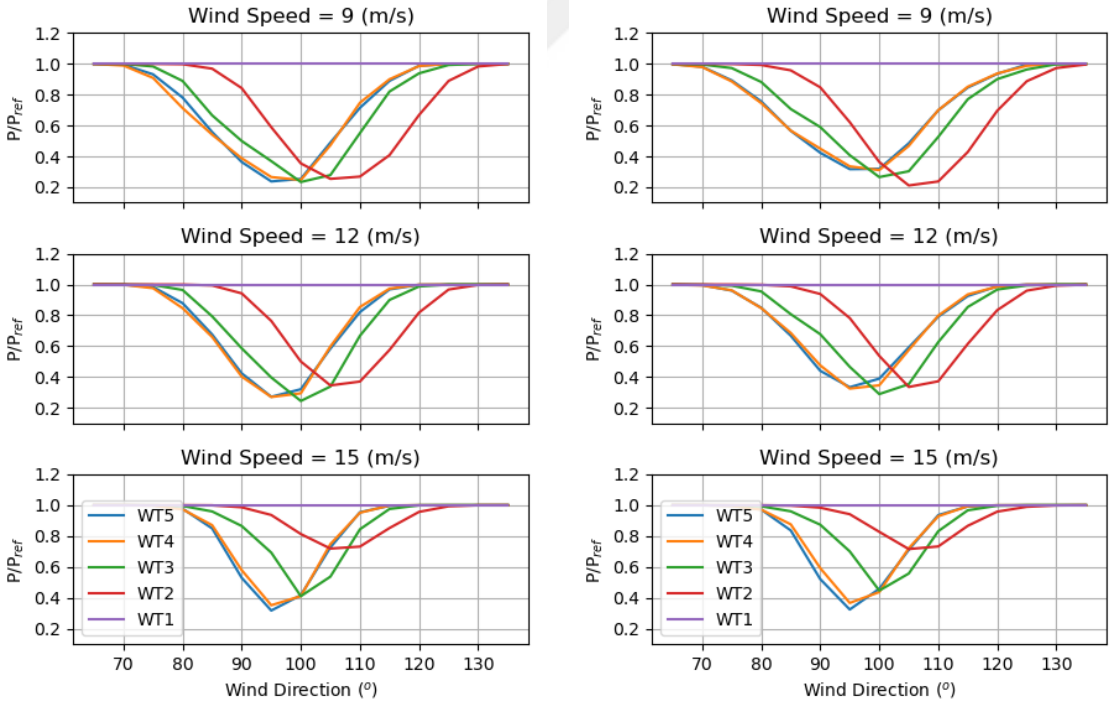

(a) Cumulative curl model. (b) Gaussian hybrid curl model.

Figure 2.13: Simulated wake losses for ESE sector winds.

For comparison purposes, the wind farm under study does not have enough data for 1^o wind direction bin representation due to wind distribution being heavily dominated by northern winds. Additionally, from calibration in Section 1.3.4, measured wind directions have 3.6^o standard deviation, meaning using higher resolution wind direction bins would not necessarily result in improvements. The complete set of wake simulations for the five different wind speeds with 1^o wind direction bins are available in Figures B.1 and B.2.

2.5 Yaw Optimization

Optimal yaw angles are calculated using the Serial Refine (SR) method available in FLORIS as described in [84]. SR method sorts the wind turbines upwind to downwind. The first pass of the optimization process sets a list of equally distant yaw angles for the wind turbines. The yaw angle resulting in the maximum production is selected and passes to the second process. The second pass would then consider another equally distant set of yaw angles near the first pass with a higher resolution. Sequential Least SQuares Programming (SLSQP) [85] is used to verify and compare to the SR method. It is observed that serial refine optimization performs similarly to the SLSQP method, and the result is plotted in Figure 2.14. SR optimizer improves the processing speed by 5000% compared to the SLSQP optimization on a standard personal computer.

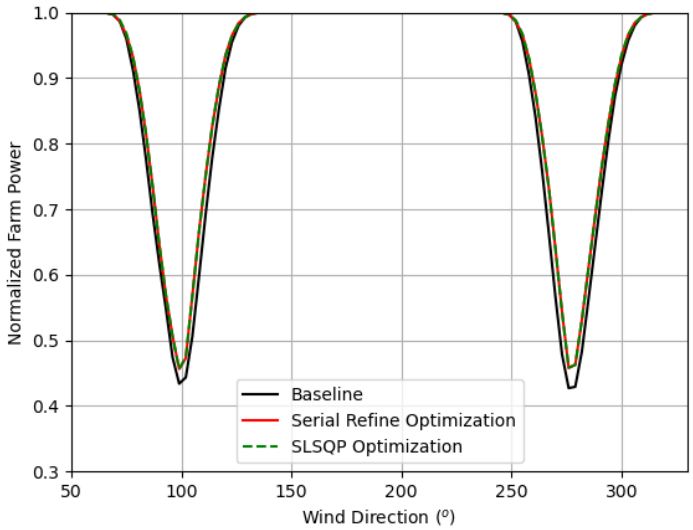

Figure 2.14: Comparison of SR and SLSQP optimization method and the baseline wake effect in the wind farm at wind speed 9 m/s.

CHAPTER 3

RESULTS AND DISCUSSION

FLORIS simulation software is used to calculate wake models for the site layout under study and the results are compared to the site wake loss measurements. Two gaussian wake models are considered for this study; the Gaussian Curl Hybrid(GCH) and the Cumulative Curl(CC) models, which are described in Section 1.4.2. Both models use the gaussian velocity deficit and curled wake for yawed conditions. The difference between the models is the wake combination method, which is essential for estimating the wake behavior of a deep array of wind turbines. The linear or sum squares approach used for earlier models lacks accuracy further downwind an array. CC model solves the flow equation for wind turbines under wake instead, while previous models used linear or root-sum-squares superposition approach for combining wake effects.

Additionally, the new CC model integrates the improvements for near-wake models to fix the near-wake expansion and increase the accuracy of far-wake considering differences for near and far-wake mixing effects. Wake loss measurements from site data are used to compare both wake models. Comparison of both models for this study using the measured and simulated wake effects for the WNW sector are depicted in Figure 3.1.

Error results for both models show that the new CC model better predicts the wake effects for an array of 5 wind turbines. Although the GCH model seems to perform better for WT3, results from the CC model are more consistent with the selection of the reference wind turbine as the foremost upwind turbine. The GCH model was tested and calibrated for arrays of 2-3 wind turbines and has performance issues for larger arrays as reported in Section 1.4.2. The CC model improvements to near-wake are visible for WT4 which is located 2.8 rotor diameters away from WT5 and has better results for the complete wind turbine array. Error is also consistent with the methodology of selecting the reference wind speed and power. For the case of the WNW sector, reference measurements are used from WT5, and further from the reference point, mean absolute error increases as expected. The measurements from multiple met masts or area measurements from a

LIDAR would improve the uncertainty. However, it is a costly investment and requires year-long measurements for the wind farm. Since the frequency of wind from the wake sectors is minimal, such investment is not feasible for most wind farms.

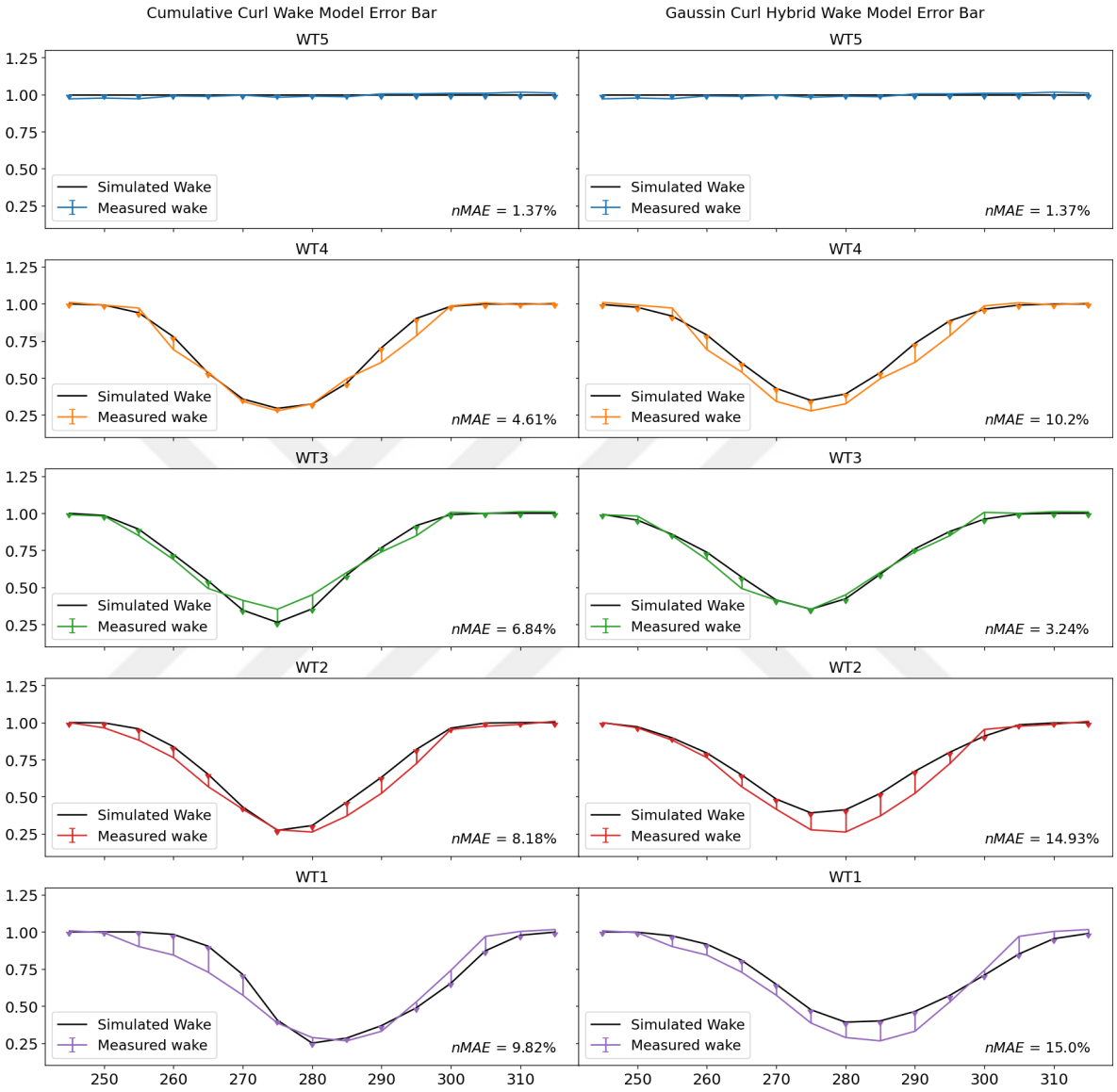

(a) Cumulative curl error bar plot. (b) Gaussian curl hybrid error bar plot.

Figure 3.1: Error bar plot of cumulative curl and gaussian hybrid curl wake models compared to measured power losses.

Optimum yaw offset angles are calculated using the serial refine optimization tool in FLORIS for the CC model. Suggested yaw offset angles are plotted against wind direction for various wind speeds, available in Figure 3.2 and 3.3. An upper limit of 25^o yaw offset

is set to limit the additional load on the wind turbine structure. Yaw misalignment of 25^o also increases the upwind wind turbine production heavily. A limit to the offset angle is used to limit uncertainty from theoretical gains even though, analytically wake steering is optimal [61]. The complete list of optimal yaw offset angles for 1 m/s wind speed steps and 2.5^o wind direction bins are generated which can be used to modify the yaw signal of the wind turbines. For wind speeds higher than 15 m/s, no yaw offset is applied since there is an abundance of kinetic energy downwind while the nominal power limits the upwind turbine. Therefore, wake steering after 15 m/s has a negligible contribution to the AEP and disabling yaw misalignment after nominal wind speeds ensure no extra load on the wind turbine structure.

The power gain from wake steering under wake conditions is simulated and plotted per wind speed step in Figure 3.4. The distribution of the AEP impact is calculated by scaling the power gain with the frequency of wind speed occurrence, which shows the maximum AEP contribution from wind speeds at 8m/s. The effect of wake steering at 8 m/s wind speed is shown in Figure 3.5. Wind farm AEP without wake losses is calculated using the 5-year average frequency of each reference wind speed bin of width $1m/s$, wind direction bin of width 5^o, and empirically derived power curves. The AEP impact of various wind speeds is shown in Figure 3.4. The wind direction bin width selection is in line width, the uncertainty related to selecting reference wind direction from 2.2.2 and the resolution of SCADA-recorded yaw angles of 1^o.

Due to the lack of recorded wind speed standard deviation measurements on SCADA, it was not possible to evaluate the effects of turbulence intensity, contributing to uncertainty in Figure 2.7. For this study, an average turbulence intensity that is the best fit for the centerline wake effect and has the lowest error value compared with the measured wake effect is used. Due to the sensitivity to turbulence intensity, it is highly recommended to simulate and calibrate the wake steering for a range of turbulence intensity values. An alternative approach to estimating turbulence intensity using minimum and maximum power values has been investigated; however, found not to be representative of the wake measurements.

The AEP of the wind farm is calculated using the average frequency of wind speed and wind direction with and without wake effects, therefore discarding the curtailment or downtime. Wind farm AEP is estimated to be 45.593 GWh without wake effects and

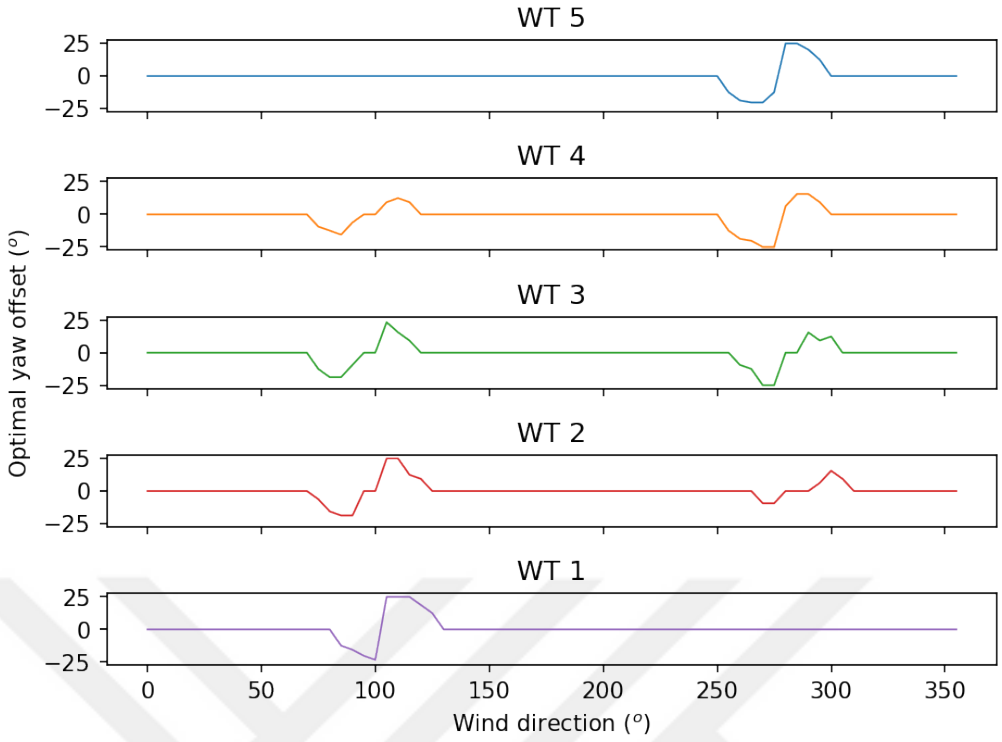

(a)

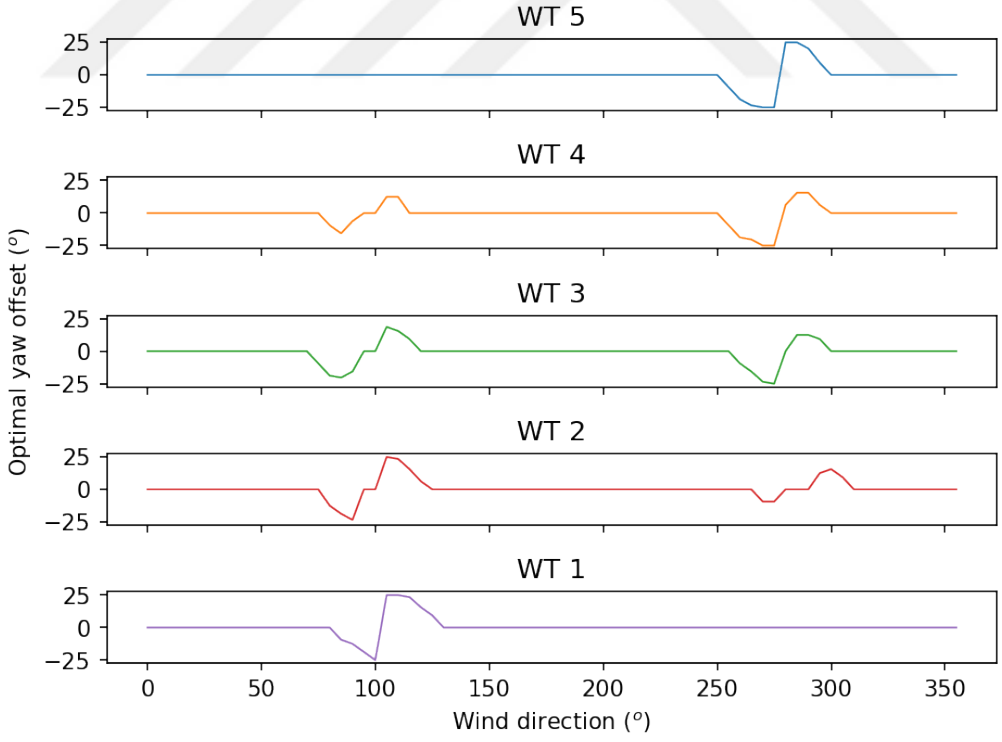

(b)

Figure 3.2: Optimal yaw offsets calculated for 6 m/s (a) and 9 m/s (b) wind speed.

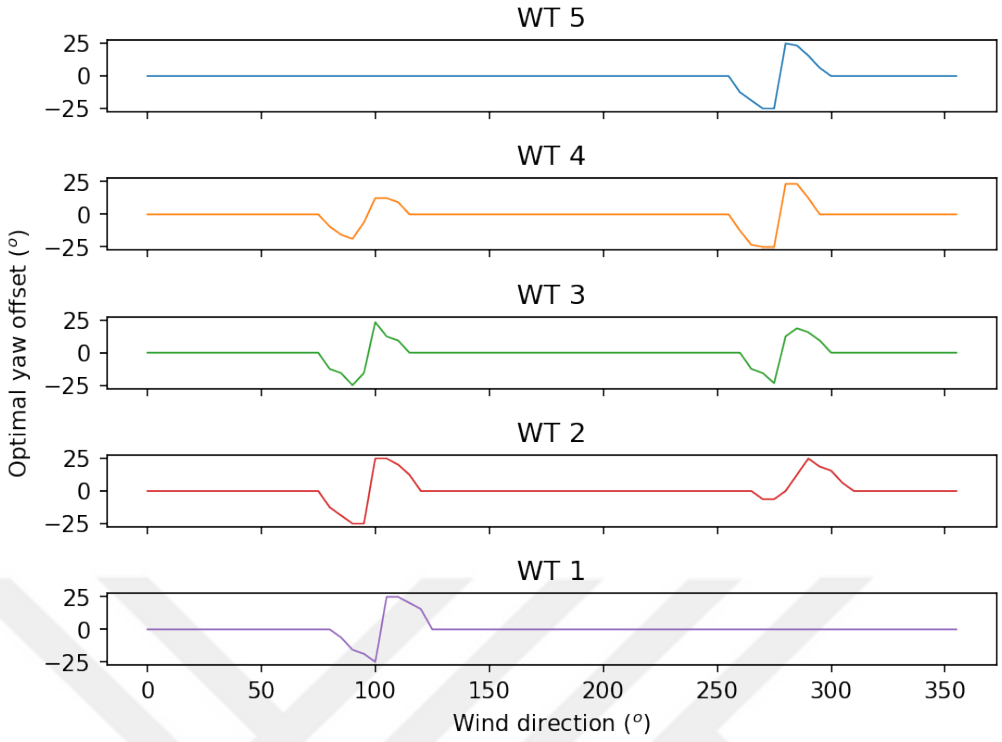

(a)

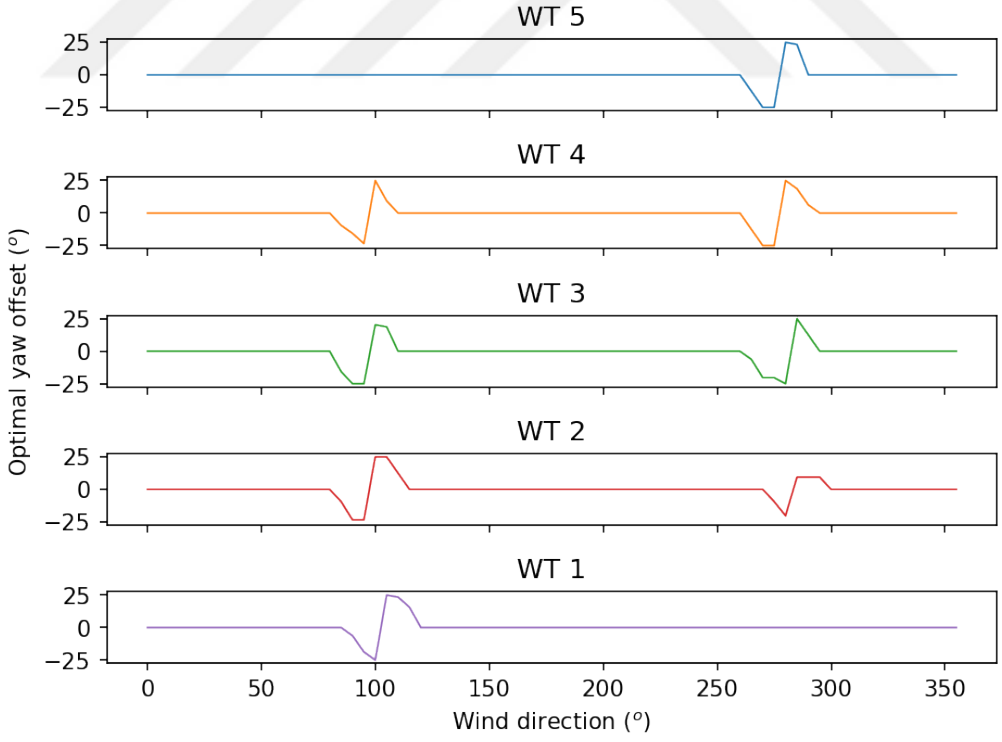

(b)

Figure 3.3: Optimal yaw offsets calculated for 12 m/s (a) and 15 m/s (b) wind speed.

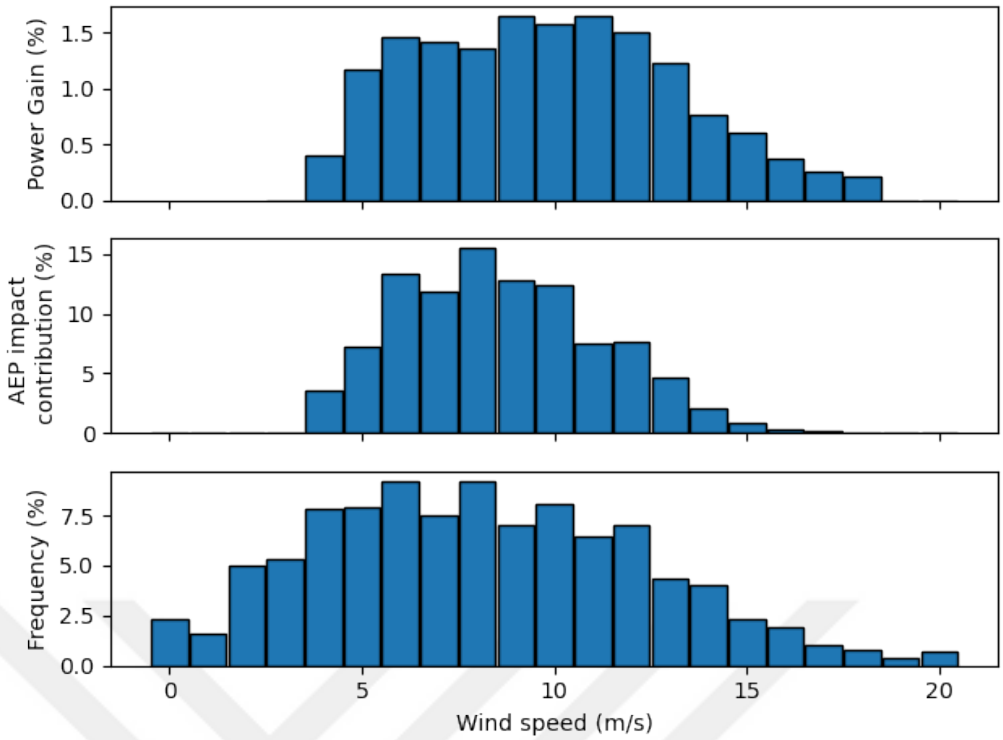

Figure 3.4: Impact of wake steering for various wind speeds when any turbine is under wake effect.

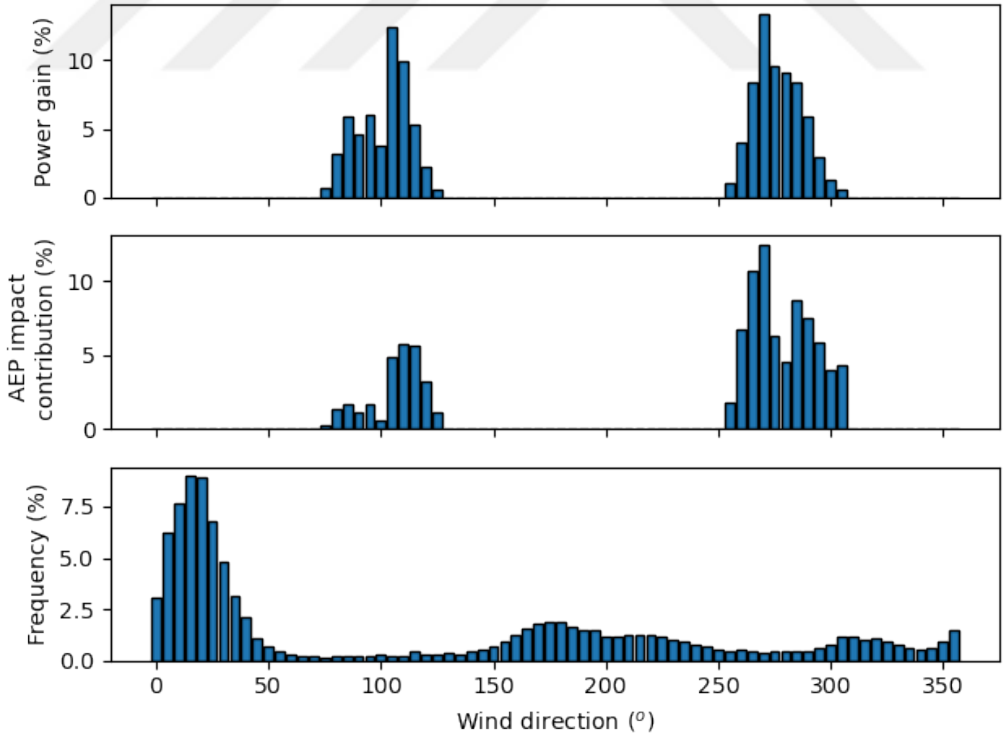

Figure 3.5: Impact of wake steering at 8m/s for the wind farm.

45.391 GWh with wake effects, as computed using the CC model. As a result of the wind farm layout, dominant wind direction, and high turbulence intensity due to complex terrain, the site experiences very low wake losses, around 0.48% in an average year. After wake steering, AEP for the site is calculated to be 45.412 GWh, which improves the wake effects by 9.59%. However, this is a minor improvement considering the wind frequency for the sectors under wake, above cut-in speed, is only 3.3% annually; it does not translate into significant AEP gain. Considering both the wind direction and wind speed frequency, AEP gain due to wake steering in this farm is calculated to be a minor 0.048%. It is essential to highlight that wake effects are already considered in the siting process. Since turbulence intensity is higher on onshore sites, and especially for complex terrain, wake mitigation is less noticeable.

CHAPTER 4

CONCLUSION AND RECOMMENDATIONS

This study analyzes 5-year-long operational wind farm data to assess the wake steering potential. Measured wake losses are compared to FLORIS simulated wake mode; then, the FLORIS environment is utilized to find optimal yaw angle offsets for various wind conditions. Finally, the simulation is run for the optimal yaw angles to analyze wake steering gain. Wake losses improved by steering the wake away from the downwind turbines using an offset to the yaw angle at the upwind turbines.

Wind turbine-specific response is especially considered since the site is curtailed due to differences in mechanical power and grid contracted power output limit. Simulations are carried out at the total mechanical power limit since the removal of the power output limit on June 1st, 2022, and the data is filtered accordingly to be able to simulate the wind farm behavior at 100% availability.

It is shown that the new cumulative curl model represents the measured wake effects better than the previous models. The calculated error is lower for the cumulative curl model, and the error propagation is more consistent with the selection of the reference wind measurements as the upwind turbine.

Overall, this study shows that analytical wake models are in line with the SCADA measurements from a wind farm. This work details how to utilize the SCADA data for an initial assessment of the wake steering application and parameterization of analytical models. A field experiment could be carried out for a site experiencing more substantial wake effects. Integration of high-frequency data acquisition from SCADA is recommended to reduce uncertainty. Since SCADA already collects data at a much higher frequency, wake steering assessment uncertainty can be improved by increasing the time resolution and keeping the records for the standard deviation of wind speed and wind direction. A better model calibration using aero-elastic code and high-frequency data is recommended to assess the potential of wake steering better. A heterogeneous inflow map can be acquired, especially for a larger wind farm, with the measurements of parallel wind turbine arrays

to accommodate terrain effects and micro-climate better.

Wake steering optimization is shown to be improving the wake loss by 9.59%. Although for this case study, wake losses are minimal due to the very low frequency of wind from the wake-inducing directions and the high mixing effect of natural turbulence at the site, it is shown that an assessment for wake steering application is possible using operational farm data. Uncertainty of the assessment can be significantly improved, provided the SCADA system keeps already-collected data at higher frequencies. A controller design is out of the scope of this study. However, wake steering integration would consider the hysteresis effects due to wind direction and speed deviations. The response time of the yaw actuator should be carefully considered to assess the realizable wake steering gains. Loads due to yaw misalignment should be studied and monitored for safety, and a safe yaw offset limit should be set in coordination with design engineers. Assessment of the wake steering can be recalculated using the actuator constraints to obtain a more realistic AEP impact.

APPENDIX A

COMMONLY REFERRED FORMULAS

AEP is calculated using the frequency of wind direction, f_{wd} and wind speed f_u as,

$$AEP = \sum_{n=1}^{N} \sum_{wd=0}^{360} \sum_{u=1}^{u_{max}} P_n(u) f_u f_{wd} 24 \cdot 365 \tag{A.1}$$

Where $P_n(u)$ matches effective wind speed to power on the power curve of the n'th wind turbine, and N is the total number of wind turbines, including the effects of velocity deficit due to wake.

Key performance metrics used in the study for the evaluation of N samples are defined as follows,

$$nRMSE = \sqrt{\sum_{1}^{N} (\frac{x_{measurement} - x_{model}}{x_{measurement}})^2} \frac{100\%}{N} \tag{A.2}$$

$$nMAE = \sum_{1}^{N} |\frac{x_{measurement} - x_{model}}{x_{measurement}}| \frac{100\%}{N} \tag{A.3}$$

APPENDIX B

SUPPLEMANTARY FIGURES

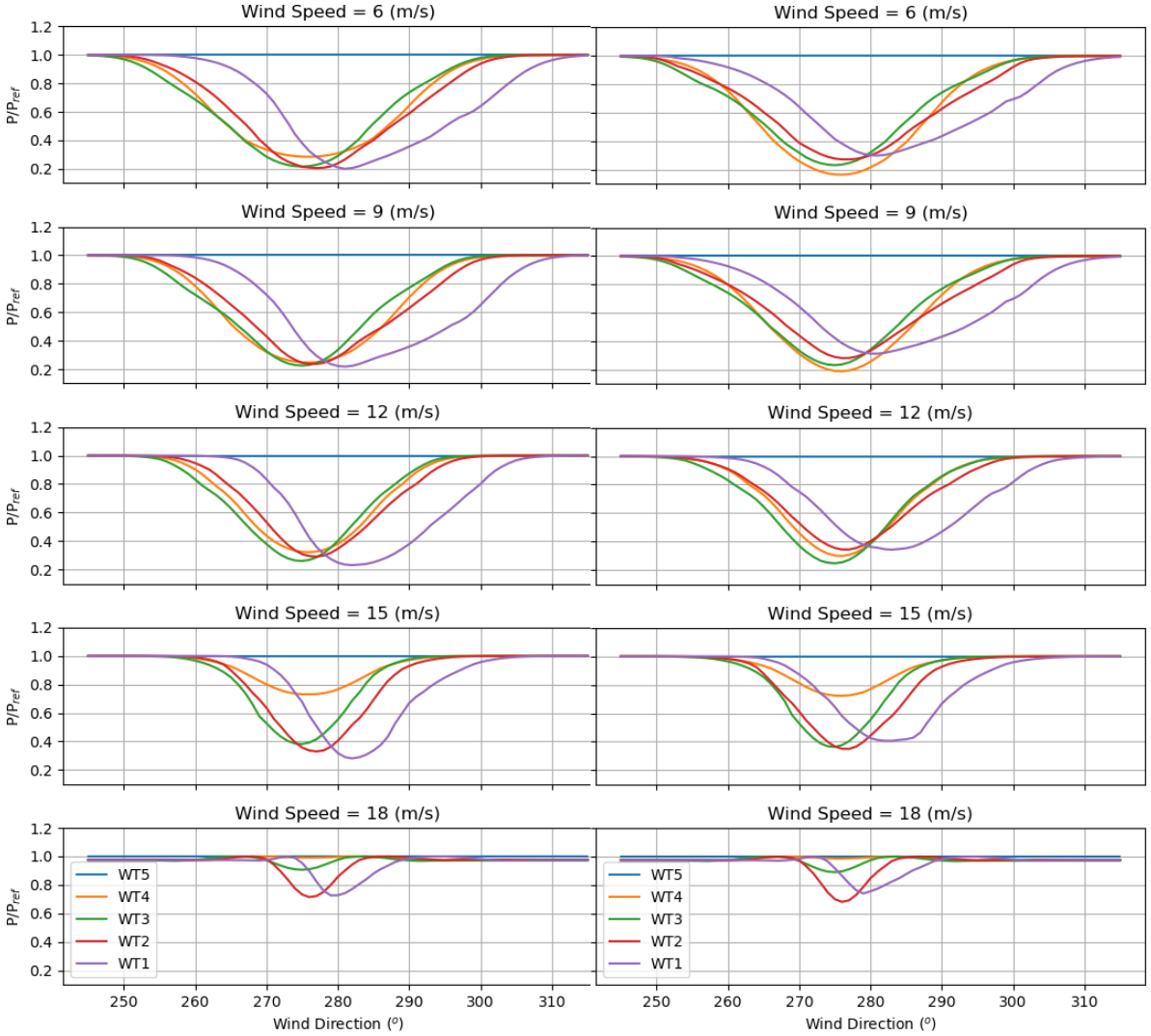

(a) Cumulative curl model.

(b) Gaussian curl model.

Figure B.1: Simulted wake losses for WNW sector winds for various wind speeds.

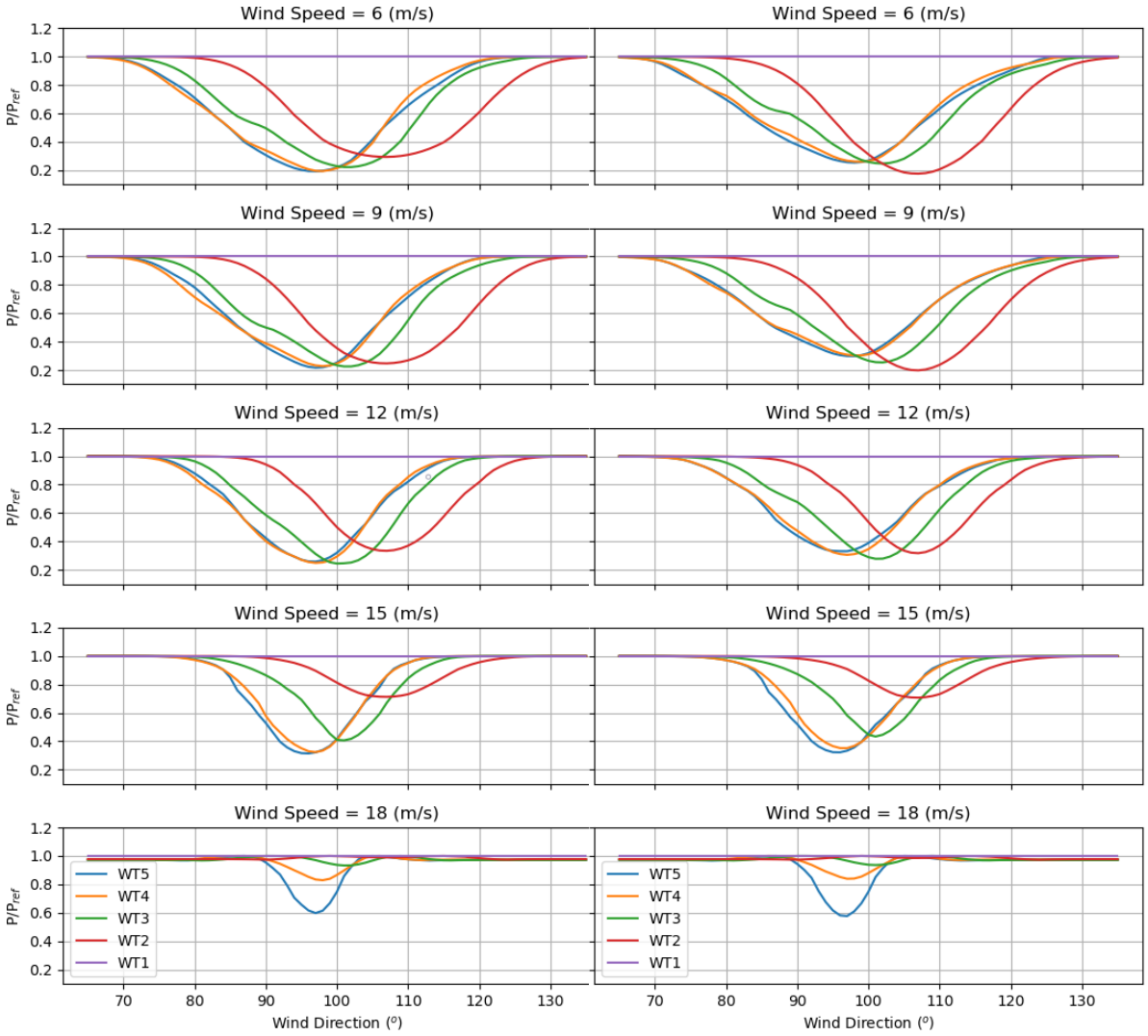

(a) Cumulative curl model.

(b) Gaussian curl model.

Figure B.2: Simulted wake losses for ESE sector winds for various wind speeds.

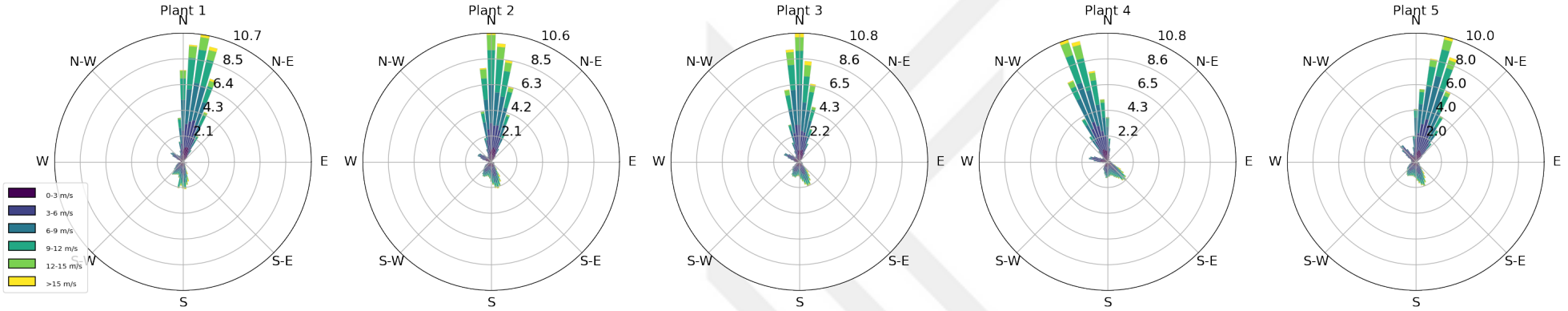

(a) Recorded yaw angle measurements.

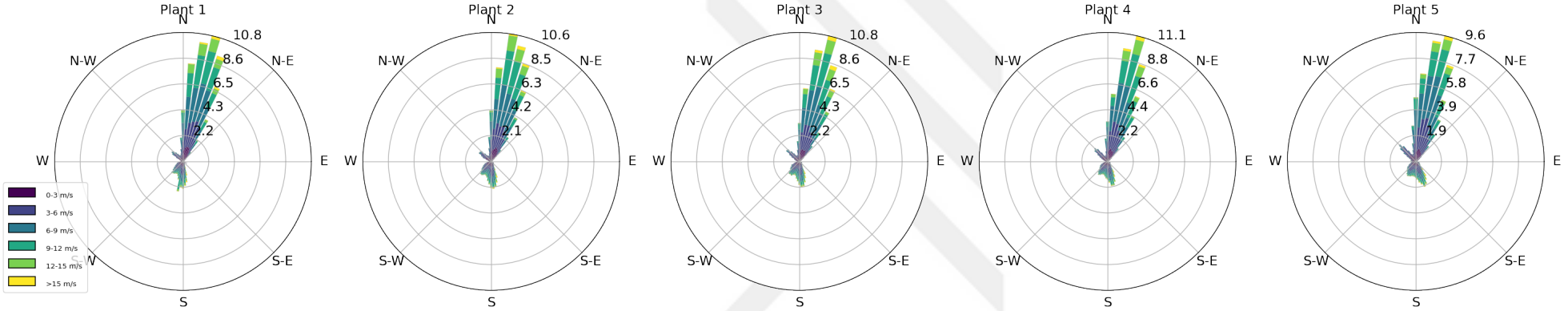

(b) Wind rose with calibrated yaw angles.

Figure B.3: Derivation of wind direction from yaw angle.

REFERENCES

[1] International Energy Agency, *World Energy Outlook 2021*. 2021, 386 pp.

[2] The International Renewable Energy Agency, *World Energy Transitions Outlook: 1.5°C Pathway*. 2022.

[3] Lazard, "Lazard's levelized cost of energy anaysis," Lazard, 15, 2021.

[4] C. L. Archer and M. Z. Jacobson, "Evaluation of global wind power," *Journal of Geophysical Research: Atmospheres*, vol. 110, D12 2005. doi: 10.1029/2004jd005462.

[5] M. Steinbuch, W. W. de Boer, O. H. Bosgra, S. A. W. M. Peters, and J. Ploeg, "Optimal control of wind power plants," *Journal of Wind Engineering and Industrial Aerodynamics*, vol. 27, no. 1, pp. 237–246, Jan. 1, 1988. doi: 10.1016/0167-6105(88)90039-6.

[6] J. Bartl and L. Sætran, "Experimental testing of axial induction based control strategies for wake control and wind farm optimization," *Journal of Physics: Conference Series*, vol. 753, p. 032 035, Sep. 2016. doi: 10.1088/1742-6596/753/3/032035.

[7] Á. Jiménez, A. Crespo, and E. Migoya, "Application of a LES technique to characterize the wake deflection of a wind turbine in yaw," *Wind Energy*, vol. 13, no. 6, pp. 559–572, 2010. doi: 10.1002/we.380.

[8] P. Fleming, J. King, K. Dykes, *et al.*, "Initial results from a field campaign of wake steering applied at a commercial wind farm – part 1," *Wind Energy Science*, vol. 4, no. 2, pp. 273–285, May 20, 2019. doi: 10.5194/wes-4-273-2019.

[9] P. Fleming, J. King, E. Simley, *et al.*, "Continued results from a field campaign of wake steering applied at a commercial wind farm – part 2," *Wind Energy Science*, vol. 5, no. 3, pp. 945–958, Jul. 24, 2020. doi: 10.5194/wes-5-945-2020.

[10] WindESCO. "WindESCO swarm press release." (Oct. 26, 2021), [Online]. Available: https://windeurope.org/ElectricCity2021/wp-content/uploads/ninja-forms/8/Swarm-Press-Release-for-Print.pdf (visited on 09/24/2022).

[11] Siemens Gamesa. "Siemens gamesa wind adapt press release." (Nov. 26, 2019), [Online]. Available: https://www.siemensgamesa.com/en-int/-/media/siemensgamesa/downloads/en/newsroom/2019/11/press-release-siemens-gamesa-wake-adapt-en.pdf (visited on 09/24/2022).

[12] NREL, *Floris. version 3.2*, 2022.

[13] International Electrotechnical Commission, *Wind energy generation systems - Part 12-1: Power performance measurements of electricity producing wind turbines*, 2nd ed. Mar. 2017.

[14] International Electrotechnical Commission, *Wind energy generation systems - Part 1: Design requirements*, 4th ed. Feb. 2019.

[15] Enercon. "Enercon product portfolio; technical data sheets." (Sep. 2018), [Online]. Available: https://www.enercon.de/fileadmin/Redakteur/Medien-Portal/broschueren/pdf/EC_Datenblaetter_WEA_en.pdf (visited on 09/24/2022).

[16] P. M. Anderson and A. Bose, "Stability simulation of wind turbine systems," *IEEE Transactions on Power Apparatus and Systems*, vol. PAS-102, no. 12, pp. 3791–3795, Dec. 1983. doi: 10.1109/tpas.1983.317873.

[17] O. Wasynczuk, D. T. Man, and J. P. Sullivan, "Dynamic behavior of a class of wind turbine generators during randon wind fluctuations," *IEEE Transactions on Power Apparatus and Systems*, vol. PAS-100, no. 6, pp. 2837–2845, Jun. 1981. doi: 10.1109/tpas.1981.316400.

[18] L. Y. Pao and K. E. Johnson, "Control of wind turbines," *IEEE Control Systems Magazine*, vol. 31, no. 2, pp. 44–62, Apr. 2011. doi: 10.1109/mcs.2010.939962.

[19] R. J. Barthelmie, S. T. Frandsen, M. N. Nielsen, S. C. Pryor, P.-E. Rethore, and H. E. Jørgensen, "Modelling and measurements of power losses and turbulence intensity in wind turbine wakes at middelgrunden offshore wind farm," *Wind Energy*, vol. 10, no. 6, pp. 517–528, 2007. doi: 10.1002/we.238.

[20] R. J. Barthelmie, K. Hansen, S. T. Frandsen, *et al.*, "Modelling and measuring flow and wind turbine wakes in large wind farms offshore," *Wind Energy*, vol. 12, no. 5, pp. 431–444, 2009. doi: 10.1002/we.348.

[21] P. A. Fleming, A. Ning, P. M. O. Gebraad, and K. Dykes, "Wind plant system engineering through optimization of layout and yaw control," *Wind Energy*, vol. 19, no. 2, pp. 329–344, Feb. 2016. doi: 10.1002/we.1836.

[22] J. K. Lundquist, K. K. DuVivier, D. Kaffine, and J. M. Tomaszewski, "Costs and consequences of wind turbine wake effects arising from uncoordinated wind energy development," *Nature Energy*, vol. 4, no. 1, pp. 26–34, Jan. 2019. doi: 10.1038/s41560-018-0281-2.

[23] P. B. S. Lissaman, “Energy effectiveness of arbitrary arrays of wind energy collection systems,” Jan. 3, 1977.

[24] T. Faxen, “Wake interaction in an array of windmills - theory and preliminary results,” *Second International Symposium on Wind Energy Systems*, vol. 1, Jan. 1978.

[25] P. B. S. Lissaman, “Energy effectiveness of arbitrary arrays of wind turbines,” *Journal of Energy*, vol. 3, no. 6, pp. 323–328, Nov. 1, 1979. doi: 10.2514/3.62441.

[26] K. Walker, N. Adams, B. Gribben, *et al.*, “An evaluation of the predictive accuracy of wake effects models for offshore wind farms,” *Wind Energy*, vol. 19, no. 5, pp. 979–996, 2016. doi: 10.1002/we.1871.

[27] N. Jensen, “A note on wind generator interaction,” Risø National Laboratory, Roskilde, Report 87-550-0971-9, 1983.

[28] “Wake effect model - WAsP.” (2021), [Online]. Available: https://www.wasp.dk/wasp/wake-effect-model (visited on 10/01/2022).

[29] J. F. Ainslie, “Calculating the flowfield in the wake of wind turbines,” *Journal of Wind Engineering and Industrial Aerodynamics*, vol. 27, no. 1, pp. 213–224, Jan. 1, 1988. doi: 10.1016/0167-6105(88)90037-2.

[30] P. E. J. Vermeulen, “Studies of the wake structure of model wind turbine generators,” TNO, Apeldoorn, 79-012904, Nov. 1979.

[31] M. Bastankhah and F. Porté-Agel, “A new analytical model for wind-turbine wakes,” *Renewable Energy*, Special issue on aerodynamics of offshore wind energy systems and wakes, vol. 70, pp. 116–123, Oct. 1, 2014. doi: 10.1016/j.renene.2014.01.002.

[32] M. Abkar and F. Porté-Agel, “Influence of atmospheric stability on wind-turbine wakes: A large-eddy simulation study,” *Physics of Fluids*, vol. 27, no. 3, p. 035 104, Mar. 2015. doi: 10.1063/1.4913695.

[33] K. A. Kragh and M. H. Hansen, “Load alleviation of wind turbines by yaw misalignment: Load alleviation of wind turbines by yaw misalignment,” *Wind Energy*, vol. 17, no. 7, pp. 971–982, Jul. 2014. doi: 10.1002/we.1612.

[34] R. Damiani, S. Dana, J. Annoni, *et al.*, “Assessment of wind turbine component loads under yaw-offset conditions,” *Wind Energy Science*, vol. 3, no. 1, pp. 173–189, Apr. 13, 2018. doi: 10.5194/wes-3-173-2018.

[35] M. Bastankhah and F. Porté-Agel, "Experimental and theoretical study of wind turbine wakes in yawed conditions," *Journal of Fluid Mechanics*, vol. 806, pp. 506–541, Nov. 2016. doi: 10.1017/jfm.2016.595.

[36] P. Brugger, M. Debnath, A. Scholbrock, *et al.*, "Lidar measurements of yawed-wind-turbine wakes: Characterization and validation of analytical models," *Wind Energy Science*, vol. 5, no. 4, pp. 1253–1272, Oct. 8, 2020. doi: 10.5194/wes-5-1253-2020.

[37] L. A. Martínez-Tossas, J. Annoni, P. A. Fleming, and M. J. Churchfield, "The aerodynamics of the curled wake: A simplified model in view of flow control," *Wind Energy Science*, vol. 4, no. 1, pp. 127–138, Mar. 5, 2019. doi: 10.5194/wes-4-127-2019.

[38] K. Gunn, C. Stock-Williams, M. Burke, *et al.*, "Limitations to the validity of single wake superposition in wind farm yield assessment," *Journal of Physics: Conference Series*, vol. 749, p. 012 003, Sep. 2016. doi: 10.1088/1742-6596/749/1/012003.

[39] B. M. Doekemeijer, E. Simley, and P. Fleming, "Comparison of the gaussian wind farm model with historical data of three offshore wind farms," *Energies*, vol. 15, no. 6, p. 1964, Jan. 2022. doi: 10.3390/en15061964.

[40] C. J. Bay, P. Fleming, B. Doekemeijer, J. King, M. Churchfield, and R. Mudafort, "Addressing deep array effects and impacts to wake steering with the cumulative-curl wake model," *Wind Energy Science Discussions*, pp. 1–28, Mar. 1, 2022. doi: 10.5194/wes-2022-17.

[41] M. Bastankhah, B. L. Welch, L. A. Martínez-Tossas, J. King, and P. Fleming, "Analytical solution for the cumulative wake of wind turbines in wind farms," *Journal of Fluid Mechanics*, vol. 911, A53, Mar. 2021. doi: 10.1017/jfm.2020.1037.

[42] F. Blondel and M. Cathelain, "An alternative form of the super-gaussian wind turbine wake model," *Wind Energy Science*, vol. 5, no. 3, pp. 1225–1236, Sep. 28, 2020. doi: 10.5194/wes-5-1225-2020.

[43] G.-W. Qian and T. Ishihara, "A new analytical wake model for yawed wind turbines," *Energies*, vol. 11, no. 3, p. 665, Mar. 2018. doi: 10.3390/en11030665.

[44] F. Bingöl, "Comparison of weibull estimation methods for diverse winds," *Advances in Meteorology*, vol. 2020, e3638423, Jul. 6, 2020. doi: 10.1155/2020/3638423.

[45] D. Dilip and F. Porté-Agel, "Wind turbine wake mitigation through blade pitch offset," *Energies*, vol. 10, no. 6, p. 757, Jun. 2017. doi: 10.3390/en10060757.

[46] J. Frederik, B. Doekemeijer, S. Mulders, and J.-W. v. Wingerden, "On wind farm wake mixing strategies using dynamic individual pitch control," *Journal of Physics: Conference Series*, vol. 1618, no. 2, p. 022 050, Sep. 2020. doi: 10.1088/1742-6596/1618/2/022050.

[47] P. M. O. Gebraad and J. W. van Wingerden, "Maximum power-point tracking control for wind farms," *Wind Energy*, vol. 18, no. 3, pp. 429–447, 2015. doi: 10.1002/we.1706.

[48] J. G. Schepers and S. P. v. d. Pijl, "Improved modelling of wake aerodynamics and assessment of new farm control strategies," *Journal of Physics: Conference Series*, vol. 75, p. 012 039, Jul. 2007. doi: 10.1088/1742-6596/75/1/012039.

[49] K. Boorsma, "Heat and flux. analysis of field measurements," Nov. 15, 2012.

[50] D. van der Hoek, S. Kanev, J. Allin, D. Bieniek, and N. Mittelmeier, "Effects of axial induction control on wind farm energy production - a field test," *Renewable Energy*, vol. 140, pp. 994–1003, Sep. 1, 2019. doi: 10.1016/j.renene.2019.03.117.

[51] E. Bossanyi and R. Ruisi, "Axial induction controller field test at sedini wind farm," *Wind Energy Science*, vol. 6, no. 2, pp. 389–408, Mar. 15, 2021. doi: 10.5194/wes-6-389-2021.

[52] E. Bossanyi, R. Ruisi, G. C. Larsen, and M. M. Pedersen, "Axial induction control design for a field test at lillgrund wind farm," *Journal of Physics: Conference Series*, vol. 2265, no. 4, p. 042 032, May 2022. doi: 10.1088/1742-6596/2265/4/042032.

[53] I. Eguinoa, T. Göçmen, P. B. Garcia-Rosa, *et al.*, "Wind farm flow control oriented to electricity markets and grid integration: Initial perspective analysis," *Advanced Control for Applications*, vol. 3, no. 3, e80, 2021. doi: 10.1002/adc2.80.

[54] T. Göçmen, G. Giebel, N. K. Poulsen, and P. E. Sørensen, "Possible power of down-regulated offshore wind power plants: The PossPOW algorithm," *Wind Energy*, vol. 22, no. 2, pp. 205–218, 2019. doi: 10.1002/we.2279.

[55] B. Clayton and P. Filby, "Measured effects of oblique flows and change in blade pitch angle on performance and wake development of model wind turbines," in *Proc 4th BWEA Wind Energy Conference*, 1982.

[56] J. Vermeer and J. de Boer, "Wake structure of a rotor model in yaw," in *European Community Wind Energy Conference*, 1993, pp. 8–12.

[57] I. Grant, P. Parkin, and X. Wang, "Optical vortex tracking studies of a horizontal axis wind turbine in yaw using laser-sheet, flow visualisation," *Experiments in Fluids*, vol. 23, no. 6, pp. 513–519, Dec. 1, 1997. doi: 10.1007/s003480050142.

[58] J. King, P. Fleming, R. King, *et al.*, "Control-oriented model for secondary effects of wake steering," *Wind Energy Science*, vol. 6, no. 3, pp. 701–714, May 21, 2021. doi: 10.5194/wes-6-701-2021.

[59] P. Fleming, J. Annoni, M. Churchfield, *et al.*, "A simulation study demonstrating the importance of large-scale trailing vortices in wake steering," *Wind Energy Science*, vol. 3, no. 1, pp. 243–255, May 14, 2018. doi: 10.5194/wes-3-243-2018.

[60] J. Wagenaar, L. Machielse, and J. Schepers, "Controlling wind in ECN's scaled wind farm," in *EWEA 2012*, Jan. 1, 2012.

[61] P. Fleming, J. Annoni, J. J. Shah, *et al.*, "Field test of wake steering at an offshore wind farm," *Wind Energy Science*, vol. 2, no. 1, pp. 229–239, May 8, 2017. doi: 10.5194/wes-2-229-2017.

[62] M. F. Howland, S. K. Lele, and J. O. Dabiri, "Wind farm power optimization through wake steering," *Proceedings of the National Academy of Sciences*, vol. 116, no. 29, pp. 14 495–14 500, Jul. 16, 2019. doi: 10.1073/pnas.1903680116.

[63] M. F. Howland, J. B. Quesada, J. J. P. Martínez, *et al.*, "Collective wind farm operation based on a predictive model increases utility-scale energy production," *Nature Energy*, vol. 7, no. 9, pp. 818–827, Sep. 2022. doi: 10.1038/s41560-022-01085-8.

[64] J. Annoni, P. Fleming, A. Scholbrock, *et al.*, "Analysis of control-oriented wake modeling tools using lidar field results," *Wind Energy Science*, vol. 3, no. 2, pp. 819–831, Nov. 1, 2018. doi: 10.5194/wes-3-819-2018.

[65] B. M. Doekemeijer, S. Kern, S. Maturu, *et al.*, "Field experiment for open-loop yaw-based wake steering at a commercial onshore wind farm in italy," *Wind Energy Science*, vol. 6, no. 1, pp. 159–176, Jan. 27, 2021. doi: 10.5194/wes-6-159-2021.

[66] E. Simley, P. Fleming, N. Girard, L. Alloin, E. Godefroy, and T. Duc, "Results from a wake-steering experiment at a commercial wind plant: Investigating the wind speed dependence of wake-steering performance," *Wind Energy Science*, vol. 6, no. 6, pp. 1427–1453, Nov. 12, 2021. doi: 10.5194/wes-6-1427-2021.

[67] ESRI. “Terrain: Slope map - overview.” (2022), [Online]. Available: https://www.arcgis.com/home/item.html?id=a1ba14d09df14f42ad6ca3c4bcebf3b4 (visited on 10/04/2022).

[68] International Electrotechnical Commission, *Wind energy generation systems - Part 12-2: Power performance of electricity-producing wind turbines based on nacelle anemometry*, 2nd ed. IEC, Mar. 2013.

[69] K. S. Hansen, R. J. Barthelmie, L. E. Jensen, and A. Sommer, “The impact of turbulence intensity and atmospheric stability on power deficits due to wind turbine wakes at horns rev wind farm,” *Wind Energy*, vol. 15, no. 1, pp. 183–196, 2012. doi: 10.1002/we.512.

[70] N. Mittelmeier, J. Allin, T. Blodau, *et al.*, “An analysis of offshore wind farm SCADA measurements to identify key parameters influencing the magnitude of wake effects,” *Wind Energy Science*, vol. 2, no. 2, pp. 477–490, Oct. 18, 2017. doi: 10.5194/wes-2-477-2017.

[71] D. Infield and G. Zorzi, “Stability impact on wake development in moderately complex terrain,” *Journal of Physics: Conference Series*, vol. 854, p. 012 024, May 2017. doi: 10.1088/1742-6596/854/1/012024.

[72] Vestas. “Vestas power uprate,” Fleet Optimisation. (2017), [Online]. Available: https://www.vestas.de/content/dam/vestas-com/de/Power_Uprate_DE_2017.pdf.coredownload.inline.pdf (visited on 10/08/2022).

[73] EPIAS and TEIAS. “Gerçek zamanlı üretim - gerçekleşen üretim - üretim | EPİAŞ şeffaflık platformu.” (2022), [Online]. Available: https://seffaflik.epias.com.tr/transparency/uretim/gerceklesen-uretim/gercek-zamanli-uretim.xhtml (visited on 10/29/2022).

[74] EPIAS and TEIAS. “Uzlaştırma esas veriş miktarı - gerçekleşen üretim - üretim | EPİAŞ şeffaflık platformu.” (2022), [Online]. Available: https://seffaflik.epias.com.tr/transparency/uretim/gerceklesen-uretim/uevm.xhtml (visited on 10/29/2022).

[75] P. M. O. Gebraad, F. W. Teeuwisse, J. W. van Wingerden, *et al.*, “Wind plant power optimization through yaw control using a parametric model for wake effects—a CFD simulation study,” *Wind Energy*, vol. 19, no. 1, pp. 95–114, 2016. doi: 10.1002/we.1822.

[76] B. M. Doekemeijer, D. van der Hoek, and J.-W. van Wingerden, “Closed-loop model-based wind farm control using FLORIS under time-varying inflow

conditions," *Renewable Energy*, vol. 156, pp. 719–730, Aug. 1, 2020. doi: 10.1016/j.renene.2020.04.007.

[77] J. Schreiber, E. M. Nanos, F. Campagnolo, and C. L. Bottasso, "Verification and calibration of a reduced order wind farm model by wind tunnel experiments," *Journal of Physics: Conference Series*, vol. 854, no. 1, p. 012 041, May 2017. doi: 10.1088/1742-6596/854/1/012041.

[78] F. Campagnolo, R. Weber, J. Schreiber, and C. L. Bottasso, "Wind tunnel testing of wake steering with dynamic wind direction changes," *Wind Energy Science*, vol. 5, no. 4, pp. 1273–1295, Oct. 8, 2020. doi: 10.5194/wes-5-1273-2020.

[79] S. Gomez-Iradi, D. Astrain, M. Aparicio, L. Fernández, and R. Chávez, "Numerical validation of wind plant control strategies," *Journal of Physics: Conference Series*, vol. 1618, no. 2, p. 022 010, Sep. 2020. doi: 10.1088/1742-6596/1618/2/022010.

[80] F. Campagnolo, L. Imširović, R. Braunbehrens, and C. L. Bottasso, "Further calibration and validation of FLORIS with wind tunnel data," *Journal of Physics: Conference Series*, vol. 2265, no. 2, p. 022 019, May 2022. doi: 10.1088/1742-6596/2265/2/022019.

[81] I. Katic, J. Højstrup, and N. Jensen, "A simple model for cluster efficiency," English, in *EWEC'86. Proceedings. Vol. 1*, W. Palz and E. Sesto, Eds., European Wind Energy Association Conference and Exhibition, EWEC '86 ; Conference date: 06-10-1986 Through 08-10-1986, A. Raguzzi, 1987, pp. 407–410.

[82] P. M. O. Gebraad, "Data-driven wind plant control," 2014.

[83] N. G. Nygaard, S. T. Steen, L. Poulsen, and J. G. Pedersen, "Modelling cluster wakes and wind farm blockage," *Journal of Physics: Conference Series*, vol. 1618, no. 6, p. 062 072, Sep. 2020. doi: 10.1088/1742-6596/1618/6/062072.

[84] P. A. Fleming, A. P. J. Stanley, C. J. Bay, *et al.*, "Serial-refine method for fast wake-steering yaw optimization," *Journal of Physics: Conference Series*, vol. 2265, no. 3, p. 032 109, May 2022. doi: 10.1088/1742-6596/2265/3/032109.

[85] "Sequential quadratic programming," in *Numerical Optimization*. New York, NY: Springer New York, 2006, pp. 529–562. doi: 10.1007/978-0-387-40065-5_18.